DOE/ET/23144-81/1
(DE83000333)
Distribution Category UC-60

THE RESPONSE SENSITIVITY OF WIND TURBINES TO ATMOSPHERIC TURBULENCE

R. W. Thresher
W. E. Holley

Oregon State University
Mechanical Engineering Department
Corvallis, Oregon 97331

May 1981

Prepared for
Pacific Northwest Laboratory
Richland, Washington 99352 under
Prime Contract No. DE-AC06-76RLO 1830
Task Agreement DE-AT06-79ET23144
With the Department of Energy
Office of Solar Power Applications
Wind Energy Technology Division

Pacific Northwest Laboratory
Richland, Washington 99352

Blank Page

ACKNOWLEDGEMENTS

This research was supported by the U.S. Department of Energy through Battelle, Pacific Northwest Laboratory. The authors would like to thank Dr. J.R. Connell for his helpful and enthusiastic support, and the many valuable suggestions made by the PNL staff. In addition, the authors would like to acknowledge Mr. Nozar Jafarey and Mr. S-R Lin who assisted with the modeling and performed the necessary computations. The authors are indebted to Ms. Laurie Campbell for her many hours of effort spent putting the report into final form.

Figure		Page
4.6	Mod-G power spectral density of thrust force, F_y.	69
4.7	Mod-G power spectral density of yaw moment, M_z.	70
4.8	Mod-G power spectral density of pitch moment, M_x.	71
4.9	Mod-M power spectral density of power output using the frozen wake.	72
4.10	Mod-M power spectral density of power output using the equilibrium wake.	73
4.11	Mod-G power spectral density of power output using the frozen wake.	74
4.12	Mod-G power spectral density of power output using the equilibrium wake.	75
4.13	The effect of the gradients, $v_{y,x}$ and $v_{y,z}$ on thrust for Mod-M using the equilibrium wake.	76
4.14	The effect of the gradients $v_{y,x}$ and $v_{y,z}$ on yaw angle for Mod-M using the equilibrium wake.	77
4.15	The effect of the gradients $v_{y,x}$ and $v_{y,z}$ on pitch moment for Mod-M using the equilibrium wake.	78
4.16	The effect of the gradients $v_{y,x}$ and $v_{y,z}$ on the side force for Mod-G using the equilibrium wake.	79
4.17	The effect of the gradients $v_{y,x}$ and $v_{y,z}$ on thrust for the Mod-G using the equilibrium wake.	80
4.18	The effect of the gradients $v_{y,x}$ and $v_{y,z}$ on yaw moments for Mod-G using the equilibrium wake.	81

LIST OF FIGURES

Figure		Page
2.1	Streamlines for in-plane velocity gradient terms.	20
2.2	Dimensionless parameter a_* for uniform turbulence terms.	21
2.3	Dimensionless parameter b_* for uniform turbulence terms.	22
2.4	Dimensionless parameter a_* for gradient turbulence terms.	23
2.5	Dimensionless parameter b_* for gradient turbulence terms.	24
2.6	Coordinate system for rotating observer.	25
2.7	Power spectral density for V_y.	26
2.8	Power spectral density for V_x and V_z.	27
2.9	Power spectral density for $V_{y,x}$ and $V_{y,z}$.	28
2.10	Power spectral density for γ_{xz}.	29
2.11	Power spectral density for ε_r and $\bar{\gamma}_r$.	30
2.12	Power spectral density for $\bar{\varepsilon}_{xz}$.	31
3.1	The turbine model.	48
3.2	Rotor geometry.	49
3.3	Blade element aerodynamic forces.	50
4.1	Mod-M power spectral density of side force, F_x.	64
4.2	Mod-M power spectral density of thrust, F_y.	65
4.3	Mod-M power spectral density of yaw angle, ϕ.	66
4.4	Mod-M power spectral density of pitch moment, M_x.	67
4.5	Mod-G power spectral density of side force, F_x.	68

Figure		Page
4.6	Mod-G power spectral density of thrust force, F_y.	69
4.7	Mod-G power spectral density of yaw moment, M_z.	70
4.8	Mod-G power spectral density of pitch moment, M_x.	71
4.9	Mod-M power spectral density of power output using the frozen wake.	72
4.10	Mod-M power spectral density of power output using the equilibrium wake.	73
4.11	Mod-G power spectral density of power output using the frozen wake.	74
4.12	Mod-G power spectral density of power output using the equilibrium wake.	75
4.13	The effect of the gradients, $v_{y,x}$ and $v_{y,z}$ on thrust for Mod-M using the equilibrium wake.	76
4.14	The effect of the gradients $v_{y,x}$ and $v_{y,z}$ on yaw angle for Mod-M using the equilibrium wake.	77
4.15	The effect of the gradients $v_{y,x}$ and $v_{y,z}$ on pitch moment for Mod-M using the equilibrium wake.	78
4.16	The effect of the gradients $v_{y,x}$ and $v_{y,z}$ on the side force for Mod-G using the equilibrium wake.	79
4.17	The effect of the gradients $v_{y,x}$ and $v_{y,z}$ on thrust for the Mod-G using the equilibrium wake.	80
4.18	The effect of the gradients $v_{y,x}$ and $v_{y,z}$ on yaw moments for Mod-G using the equilibrium wake.	81

NOMENCLATURE

a	Distance between tower center line to center of rotor.
a'	Sectional lift curve slope.
a_*	Dimensionless wind parameter.
$[A]$	System dynamics matrix (augmented system).
$[A_w]$	System dynamics matrix (wind system).
$A'(\bar{r})$	Aerodynamic coefficient.
b_*	Dimensionless wind parameter.
$[B]$	Input distribution matrix (augmented system).
$[B_w]$	Input distribution matrix (wind system).
$B'(\bar{r})$	Aerodynamic coefficient.
$c(\bar{r})$	Local airfoil chord.
c_g	Generator torque coefficient.
$[c]$	Response matrix.
c_t	Chord at rotor tip.
C_{D_0}	Zero-lift drag coefficient.
$[C]$	Turbine system damping matrix.
C_L	Sectional lift coefficient.
$C'(\bar{r})$	Aerodynamic coefficient.
D	Rotor disk diameter.
$D'(\bar{r})$	Aerodynamic coefficient.
$EI(z)$	Stiffness per unit length of tower.
$E'(\bar{r})$	Aerodynamic coefficient.
$[F]$	Wind input matrix.

$F'(\bar{r})$	Aerodynamic coefficient.
h	Hub radius.
$[H_{yw}(\omega)]$	Transfer function matrix.
I_r	Total effective inertia of all the spinning mass.
$[k]$	Tower stiffness matrix.
$[K]$	Turbine system stiffness matrix.
χ_d	Lift deficiency factor (see 3.5).
χ_a	Added lift factor (see 3.5).
L	Turbulence integral scale.
L_t	Tower height.
$[m]$	Tower inertia matrix.
$m(z)$	Mass per unit length of tower.
$[M]$	Turbine system inertia matrix.
P	Power output.
$P_v(z)$	Interpolating polynomial.
$P_x(x)$	Interpolating polynomial.
Q	Mean torque.
$\{Q_1\}$	Steady state input vector.
r	Radial position on the rotor disk.
$\bar{r}$	r/R
R	Rotor disk radius.
$\{S_u(\omega)\}$	Power spectral density of the wind inputs.
$\{S_w\}$	Power spectral density of white noise.
$\{S_y(\omega)\}$	Power spectral density of the response.
t	Time.
T	Mean thrust.

$\{u\}$	Wind input vector.
U	Lateral translation in the x direction.
$\{v_i\}$	Induced velocity vector.
$v(z,t)$	Tower deformation about one bending axis.
V	Fore aft translation in y direction.
V_i	Fluctuation components of the wind input.
$V_{i,j}$	Turbulence gradients of the wind input.
V_{rel}	Relative wind velocity as observed from the turbine blade.
V_w	Mean wind speed.
V_∞	Wind velocity.
w	Nondimensional white noise.
x	Lateral coordinate.
$\{x\}$	Augmented system state vector.
$\{X\}$	Tower displacement coordinate vector.
y	Longitudinal coordinate.
$\{y\}$	System response vector.
z	Vertical coordinate.
α	Blade angle of attack.
β_o	Static coning angle.
$\bar{\gamma}_r$	Defined by Eq. 3.
γ_{xz}	Swirl about mean wind axis (in plane turbulence input)
$\bar{\gamma}_{xz}$	In plane shear strain rate (turbulence input).
ε_r	Defined by Eq. 3.

ε_{xz}	In plane shear strain rate (turbulence input).
$\bar{\varepsilon}_{xz}$	In plane dilation (turbulence input).
η	The ratio C_{D_0}/a'.
η_e	Overall power conversion efficiency.
$\theta(\bar{r})$	Blade pitch setting.
λ	$V_w/R\Omega$.
μ	Blade coordinate in the plane of rotation and normal ξ.
ν	Blade coordinate normal to the rotor disk.
ξ	Spanwise blade coordinate.
ρ	Density of air.
σ^2	Turbulent velocity component variance.
ϕ	Nacelle yaw angle.
χ	Nacelle pitch angle.
ψ	Azimuthal angular position of a rotor blade.
ω	Frequency in radians/sec.
Ω	Mean rotation rate.

TABLE OF CONTENTS

	Page
CHAPTER 1. INTRODUCTION	1
1.1 Background	1
1.2 Past Approaches	2
1.3 The Goal of This Report	6
1.4 References	7
CHAPTER 2. TURBULENCE INPUTS	8
2.1 Introduction	8
2.2 Model Assumptions and Approximations	9
2.3 Model Description	11
2.4 Rotating Reference Frame for In-Plane Terms	14
2.5 Typical Wind Turbine Cases	15
2.6 References	17
CHAPTER 3. THE TURBINE MODEL	32
3.1 Introduction	32
3.2 The Turbine Model	32
3.3 The Tower	33
3.4 Aerodynamic Forces	35
3.5 The Induced Velocity	40
3.6 State Space Equations	43
3.7 References	46
CHAPTER 4. MODELING RESULTS	51
4.1 Introduction	51
4.2 Response of a Small Turbine	51
4.3 Response of a Large Turbine	54
4.4 Power Output	54
4.5 The Key Turbulence Inputs	58
4.6 Conclusions and Recommendations	62
4.7 References	63
APPENDIX - Turbine System Equations	82

Blank Page

ABSTRACT

This report examines the dynamic response of wind turbines to atmospheric turbulence. The modeling handles both the wind inputs and the resulting loads using the analysis techniques of random vibration theory and spectral analysis. The report presents typical response results for a small, 8kW wind turbine and a large, 2.5 MW turbine. The turbine system mechanical model employs 5 degrees-of-freedom to represent the lower frequency motions of the system. The rotor is assumed to be rigid and is three bladed for simplicity. The aerodynamic forces are modeled using a simple quasi-static strip theory. The emphasis is placed on this model to identify the key turbulence imputs which are important in wind turbine design. On the basis of results computed for the two turbines modeled, it is determined that the most important turbulence imputs are the longitudinal fluctuations in the direction of the mean wind which act uniformly across the rotor disk (engulfs the rotor disk), and the across the disk gradients of the longitudinal wind fluctuations. Although each of these invokes a different machine response, they are judged to be of equal importance, because they each contribute significantly to the vibration energy of the lower system frequencies. The report presents numerous spectral density plots for the various turbine system responses, and discusses the results in some detail. This research effort is only one of a number of studies investigating the response of wind system to atmospheric turbulence sponsored through Pacific Northwest Laboratory.

CHAPTER 1. INTRODUCTION

1.1 Background

Since 1973, it has been the objective of the Federal Wind Energy Program to accelerate the development of reliable and economical wind energy systems to enable the earliest possible commercialization of wind power. To achieve this end, the development of a sound technological base is required. Responsibility for developing the technology base for large, horizontal-axis wind turbines was assigned to the NASA Lewis Research Center. NASA was funded to further wind technology as follows:

a) Design, build and operate an experimental turbine for research purposes, designated the Mod-0.

b) Initiate studies of wind turbines for utility applications.

c) Undertake a program of supporting research and technology development.

These initial efforts subsequently led to the four wind turbine projects designated Mod-0A, Mod-1, Mod-2, and most recently, the Mod-5A and B which are currently being designed.

From the first operation of the Mod-0 experimental turbine, it was recognized that control of the dynamic loads is critically important. Several sources for these dynamic loads have been identified: the passing of the turbine blades through the tower wake (tower shadow), the shear of the steady wind across the rotor disk, varying gravity loads due to turbine blade

rotation, and finally atmospheric turbulence. Of these sources, the tower shadow, wind shear, and varying gravity loads are deterministic. That is, with proper dynamic modeling, the fluctuating responses are directly computable. Deterministic problems of this type are handled using standard, although complicated, analysis techniques.

The fluctuations due to atmospheric turbulence pose a more difficult problem due to their random nature. It is difficult to generate enough "typical" and "extreme" response time histories to satisfy the designer that the machine will operate properly throughout its expected lifetime. The problem is not just in the amount of computation required but in determining what excitations should properly be used. Since the fluctuations arise from structural and aerodynamic interactions among the various system components, it is not simple to say which aerodynamic excitation results in a particular fluctuating response.

1.2 Past Approaches

In developing the Mod-1 wind turbine NASA specified the basic blade design loads in the Request for Proposals (RFP). This was accomplished by setting down a set of seven load cases with their frequency of occurrence as shown in Table 1.1 (1). These load cases were established on the basis of test experience with the Mod-0 wind turbine and a dash of engineering judgment. Although this approach lifted some of the burden for developing a complete analysis from the contractor, the result was a

Table 1.1. Blade Design Loads (from Ref. 1)

Case Number	Description	Frequency of Occurrence
1	Rated power, rated wind speed.	10^8
2	Initially at rated power, wind speed increase from rated to 60 mph in 1/4 sec, no pitch change, rotor overspeed 25%.	10^5
3	Initially at rated power, change pitch angle to feather in 11 seconds.	Occasional (Proportional Limit)
4	Initially at rated power, wind speed decreased from rated to zero in 1/4 second.	10^5
5	Blades in horizontal feathered position: wind speed 120 mph from any direction.	Occasional (Proportional Limit)
6	Rotor operating at design rpm, wind speed 50 mph at 20° yaw angle, change yaw angle at 2°/sec.	10^5
7	Rotor operating at design rpm, no power, velocity retardation of 50% due to "tower shadow".	10^5

restrictive set of specifications which were difficult to modify as the design evolved, and probably encouraged a conservative design philosophy.

The Mod-2 RFP specified a turbulence model rather than a set of load cases. This left the contractor with the nontrivial task of developing the analysis methods and discovering the important load cases. The key features of the analysis procedure developed by the Boeing Company for computing the turbulence induced loads for the Mod-2 are the following:

1) The longitudinal turbulence intensity was computed by integrating the turbulence spectrum specified in the RFP between frequency limits of n_{min} and n_{max}.
2) "The upper frequency limit, n_{max}, is that which corresponds to the discrete gust having a circular cross-section which engulfs 50 percent of the disk diameter with 50 percent correlation across the separation distance of D/2. All gusts having frequencies less than n_{max} are conservatively assumed to engulf the entire rotor."
3) "The lower frequency limit, n_{min}, is computed from the wind turbine dynamic response analysis as being that which corresponds to a discrete gust which produces a variation in rotor torque less than 5 percent from its steady state value."
4) Wind turbine loads are then computed using this turbulence intensity and assuming a discrete gust with a (1-cos) shape.

For more details, the interested reader is referred to the reference (1) contractor report.

The methods for computing the loads and dynamic responses due to atmospheric turbulence for both the Mod-1 and Mod-2 have some important similarities. They both reduce the turbulence input to some type of an effective deterministic discrete gust which totally engulfs the rotor. For the Mod-1 the effective gust is based on experience with the Mod-0, while for Mod-2 the discrete gust is based on a general turbulence specification and the turbine dynamic characteristics. In addition, they both compute wind turbine loads using the effective deterministic gust as an input to a conventional analysis code. Then having the loads and an estimate of the number of occurrences, a fatigue analysis is done.

It has been the goal of this research project to develop an alternate analysis technique for determining the influence of excitations due to atmospheric turbulence. The basic approach has been to avoid the discrete deterministic gust concept and to treat both the wind input and the resulting loads using statistical methods which provide more insight into the basic physics of the wind response characteristics of wind turbines. The analysis technique developed takes advantage of the wealth of material concerning random vibrations and spectral analysis such as is found in references (3) and (4). Using this approach the wind inputs are specified in statistical terms, and the statistics of the wind turbine responses and loads can be

computed using linear system theory. The modeling methods and assumptions are reported in detail in a separate report (5). This particular report will focus on presenting some general conclusions as a result of initial sensitivity studies. It is interesting to note that in 1955 Rosenbrock (6) handled the wind inputs with a similar statistical approach for his classical stability analysis of large wind turbines with hinged blades.

1.3 The Goal of This Report

The goal of the research reported herein is to determine which of the excitation sources in the atmospheric turbulence are important in characterizing the wind turbine system responses. Previous work in determining wind turbine system responses have largely ignored this issue. In many studies, the turbulence is modeled simply as one component along the mean wind which acts uniformly across the rotor disk (engulfs the rotor disk). The goal of our work is to establish the sensitivity of the system responses to the in-plane turbulent velocity components and to the variations across the rotor disk. In this study we have endeavored to make the system dynamic model as simple as possible and still retain the essential physical characteristics. The results should be regarded as a useful first step which should be augmented in the future with experimental data and more accurate wind turbine models involving blade flexibility and more structural degrees of freedom.

1.4 References

1. Poor, R.H. and Hubbs, R.B., "The General Electric Mod-1 Wind Turbine Generator Program," Proceedings of the Workshop on Large Wind Turbine Design Characteristics and R & D Requirements: NASA Lewis Research Center, Cleveland, Ohio, April 24-26, 1979.

2. Mod-2 Wind Turbine System Concept and Preliminary Design Report, Prepared for NASA Lewis Research Center, NASA CR-159609, January 1979.

3. Crandall, S.N. and Mark, W.D., Random Vibration in Mechanical Systems, Academic Press, New York, 1963.

4. Newland, D.E., An Introduction to Random Vibrations and Spectral Analysis, Longman, New York 1975.

5. Thresher, R.W., et al., Modeling the Response of Wind Turbines to Atmospheric Turbulence, Oregon State University Report RLO/2227-81/2, 1981.

6. Rosenbrock, H.H., Vibration and Stability Problems in Large Wind Turbines Having Hinged Blades, Electrical Research Association Report C/T 113, London, England, 1955.

CHAPTER 2. TURBULENCE INPUTS

2.1 Introduction

Fluctuations in the aerodynamic forces on a wind turbine blade are generated by the relative motions of the air with respect to the blade. These relative motions are comprised of two parts: the motions of the blade and the motions of the air. The motions of the air can further be divided into the undisturbed turbulent flow and the "induced flow" due to the presence of the wind turbine wake. The terms comprising the undisturbed flow will be characterized in this chapter. More precisely, for a horizontal axis wind turbine, the aerodynamic forces are determined by the instantaneous air velocity distribution along each of the turbine blades. These blades in turn are rotating through the turbulence field which is being convected past the turbine rotor disk. It is thus necessary to characterize the wind turbulence field by a three-dimensional velocity vector which varies randomly with time and with the position in space. A complete statistical description of this turbulent velocity field requires the determination of all possible joint probability distributions between different velocity components at different times and positions in space. Clearly, such a description will not be possible without considerable simplification. The validity of the resulting simplified model will depend upon a comparison of the characteristics predicted by the model and those observed in the atmosphere and

more importantly, those observed in actual wind turbine field tests. In this chapter we will describe this model. A more detailed description of the analytical steps used to arrive at the simplified model is presented in the modeling report (1). In the following chapters the model is used to predict wind turbine response characteristics. It is hoped that these results will be verified in the near future by direct comparison with the results of actual field tests.

2.2 Model Assumptions and Approximations

For the purpose of determining wind turbine response statistics, the response variables can be characterized by a mean value and a power spectral density function. This report focuses on the determination of the latter since a great deal of attention has been placed in the literature on determining steady, wind turbine system responses (2). In order to determine the power spectral density of the system response, all of the excitation sources must be identified and characterized in terms of their respective power and cross-power spectral densities.

The wind turbulence inputs used in this report are determined in three basic modeling steps. First, the turbulent velocity field is characterized by a model which gives the correlations between velocity components at different spatial points and at different time instants. Second, the velocity field is approximated in the rotor disk by uniform and gradient components which vary with time. A correlation model for these

components is derived from the original field model. Third, simple rational spectral representations are determined which approximate the derived correlation model for the uniform and gradient components. A brief discussion of the assumptions and approximations used in these steps follows.

The turbulent velocity field is assumed to be stationary, locally homogeneous, isotropic (3) and satisfying Taylor's frozen field hypothesis (4). The Von Karman model (5) is used to characterize the correlations between velocities of spatially separated points. This model is widely used in aircraft turbulence response analysis (6,7). However, due to the anisotropic nature of the atmospheric boundary layer, the use of the model for wind turbines can be questioned. Frost (8) has estimated that the deviation from isotropy is of secondary importance. However, one should not rely heavily on design calculations which use this model until more complete experimental verification is available.

Once the correlation model of the turbulence field is established, the velocity is approximated over the rotor disk by uniform and gradient terms which vary with time. This is done to simplify the statistical nature of the random field to that of several stochastic processes. The uniform and gradient components are the first terms in an expansion and can also be recognized as terms for which aerodynamic influence coefficients are typically computed (see Chapter 3). These terms are chosen to minimize the expected error between the true velocity

and the approximate velocity over the whole rotor disk. The power spectral densities of the uniform and gradient components can then be computed. For the isotropic model, all of the cross-power spectral densities between components are zero.

In order to further simplify the model, the power spectral densities are approximated by a simple rational form, and nondimensional parameters are determined which match the low frequency power spectral density and the total variance for the computed spectra and the rational approximation. The rational form chosen corresponds to an exponentially correlated random process which is particularly easy to handle both analytically and in simulation. The following section describes the resulting model in more detail.

2.3 Model Description

Retaining uniform and gradient terms in the expansion described in the previous section, yields nine turbulence input terms which vary with time. These nine terms are described in Table 2.1. Drawings of typical fluid streamlines are shown in Figure 2.1 for the in-plane gradient terms. Each of these nine components are modeled as a stationary, exponentially correlated random process, and each of them are uncorrelated with each other. This model form is conveniently represented by the stochastic differential equation

Table 2.1 - Description of Turbulence Input Terms

Component	Description
V_x	uniform lateral or side component (in plane)
V_y	uniform longitudinal component along mean wind
V_z	uniform vertical component (in plane)
$V_{y,x}$	lateral gradient of longitudinal velocity
$V_{y,z}$	vertical gradient of longitudinal velocity
γ_{xz}	swirl about mean wind axis (in plane)
$\bar{\gamma}_{xz}$	shear strain rates (in plane)
ε_{xz}	shear strain rates (in plane)
$\bar{\varepsilon}_{xz}$	dilation (in plane)

$$\dot{u} + \hat{a}u = \hat{b}w \tag{2.1}$$

where u = instantaneous value of one of the terms $V_x, \ldots, V_{y,x}, \ldots, \gamma_{xz}$, etc.

w = nondimensional white noise with power spectral density $S_w = \sigma^2 L/V_w^3$

$$\hat{a} = \frac{V_w}{L} a_* \tag{2.2}$$

$$\hat{b} = \begin{cases} \frac{V_w^2}{L} b_* & \text{for uniform terms} \\ \frac{V_w^2}{LR} b_* & \text{for gradient terms} \end{cases} \tag{2.3}$$

σ^2 = turbulent velocity component variance

L = turbulence integral scale

V_w = mean wind speed

R = rotor disk radius

The nondimensional terms a_* and b_* are found from Figures 2.2-2.5 (as appropriate) and depend on the ratio of turbine size to turbulence scale (R/L). Power spectral densities can be obtained if desired from the equation

$$S_u(\omega) = \frac{\hat{b}^2 S_w}{\hat{a}^2 + \omega^2} \tag{2.4}$$

where ω = radian frequency.

2.4 Rotating Reference Frame for In-Plane Terms

The following pairs of turbulence input terms can be considered as components of a two-dimensional vector in the plane of the rotor disk:

1. (V_x, V_z)
2. $(V_{y,x}, V_{y,z})$
3. $(\bar{\gamma}_{xz}, \varepsilon_{xz})$

The following arguments apply equally to any of these component pairs but for simplicity only the pair (V_x, V_z) will be treated. Suppose it is necessary to model the components of this vector as seen by a rotating observer. Thus, consider the axes x' and z' which rotate at the rate Ω with respect to the original axes x and z as shown in Figure 2.6. In this case,

$$V_z' = V_z \cos\Omega t + V_x \sin\Omega t$$

$$V_x' = -V_z \sin\Omega t + V_x \cos\Omega t \qquad (2.5)$$

Since the original turbulence field was assumed to be isotropic, the terms V_x and V_z are uncorrelated and have identical power spectral densities. Thus, using the model of the previous section

$$\dot{V}_z + \hat{a}V_z = \hat{b}w_z$$

$$\dot{V}_x + \hat{a}V_x = \hat{b}w_x \qquad (2.6)$$

where w_x and w_z are uncorrelated white noise with equal power spectral densities, S_w.

Differentiating (2.5) and substituting in (2.6) yields

$$\dot{V}'_z + \hat{a}V'_z - \Omega V'_x = \hat{b}w'_z$$

$$\dot{V}'_x + \Omega V'_z + \hat{a}V'_x = \hat{b}w'_x \qquad (2.7)$$

where

$$w'_z = w_z \cos\Omega t + w_x \sin\Omega t$$

$$w'_x = -w_z \sin\Omega t + w_x \cos\Omega t \qquad (2.8)$$

Since w_x and w_z are white noise with identical power spectral densities, it is easily shown (9) that w'_x and w'_z have the same statistical properties, namely that they are uncorrelated white noise and have power spectral densities, S_w. Using Eqs. (2.7) avoids the bothersome time varying coefficients occurring in Eqs. (2.5).

2.5 Typical Wind Turbine Cases

In order to demonstrate the differences due to size, two typical wind turbines were modeled. The turbulence parameters chosen for these two cases are shown in Table 2.2. Both wind turbines have three blades, and, due to the three-bladed sums for the aerodynamic forces, only the in-plane terms $\bar{\gamma}_{xz}$ and ε_{xz} are affected by the rotating aerodynamic coordinate frame.

Table 2.2 - Parameters for Typical Wind Turbines

	Mod M	Mod G
Radius of Rotor Disk, R (ft)	16.67	150
Rated Power	8 kW	2.5 MW
Windspeed, V_w (mph)	16.63	20
Rotation Rate, Ω (rpm)	73.35	17.5
Turbulence Scale, L (ft)	300	500

This effect appears as a rotation at three times the rotor rate (see Section 3.6).

Table 2.3 contains the model parameters for the two cases. These parameters are obtained from the data in Figures 2.2-2.5 multiplied by the necessary turbulence parameters from Eqs. (2.2) and (2.3).

Figures 2.7-2.12 show the resulting power spectral densities. Note the effect of the rotating frame at three times the rotor frequency in Figure 2.11. A sharp peak occurs at this frequency, and is explained by considering that a slowly varying vector in the fixed reference frame appears to be rapidly rotating at the effective rotation rate in the rotating frame.

The models for these two cases are used in conjunction with the dynamic model of the wind turbine system to generate the results discussed in Chapter 4.

2.6 References

1. Thresher, et al., Modeling the Response of Wind Turbines to Atmospheric Turbulence, Oregon State University Report No. RL0/2227-81/2 (1981).
2. Wilson, R.E., Lissaman, P.B.S. and Walker, S.N., Aerodynamic Performance of Wind Turbines, Oregon State University, Dept. of Mechanical Engineering (1976).
3. Batchelor, G.K., The Theory of Homogeneous Turbulence, Cambridge (1953), pp. 169-187.

Table 2.3 - Turbulence Model Parameters

		Mod M (8kW)	Mod G (2.5 MW)
	S_w (s.)	.085415	.11837
V_y	$\hat{a}(s^{-1})$	.071073	.040053
	$\hat{b}(ft/s^2)$	2.4389	1.5615
V_x, V_z	$\hat{a}(s^{-1})$	.14477	.085170
	$\hat{b}(ft/s^2)$	3.5143	2.3767
$V_{y,x}, V_{y,z}$	$\hat{a}(s^{-1})$	.53924	.093732
	$\hat{b}(s^{-2})$	.23787	.011101
γ_{xz}	$\hat{a}(s^{-1})$	.73005	.13147
	$\hat{b}(s^{-2})$	.13737	.010941
$\bar{\gamma}_{xz}, \varepsilon_{xz}$	$\hat{a}(s^{-1})$	.91179	.16779
	$\hat{b}(s^{-2})$	.12294	.0099405
$\bar{\varepsilon}_{xz}$	$\hat{a}(s^{-1})$	7.6271	2.8245
	$\hat{b}(s^{-2})$	.23609	.027480

4. Taylor, G.I., "Eddy Motion in the Atmosphere," Phil. Trans. of the Royal Soc., London, vA215 (1915), pp. 14-22.

5. Von Karman, T., "Sur la Theorie Statistique de la Turbulence," Comptes Rendus de Scanies de l'Academie de Sciences, v. 222 (1948), pp. 2108-2111.

6. Holley, W.E. and Bryson, A.E., Wind Modeling and Lateral Aircraft Control for Automatic Landing, Stanford University, Dept. of Aeronautics and Astronautics, Rept. No. 489 (1975), pp. 1-15.

7. Eichenbaum, F.D., "A General Theory of Aircraft Response to Three Dimensional Turbulence," J. of Aircraft, v. 8, n. 5 (1971), pp. 353-360.

8. Frost, W. and Lin, M.-C., "Two-Dimensional Turbulence Models," Proc. 2nd DOE/NASA Wind Turbine Dynamics Workshop, Cleveland, Ohio, Feb. 24-26, 1981.

9. Papoulis, A., Probability, Random Variables, and Stochastic Processes, McGraw-Hill (1965), pp. 373-374.

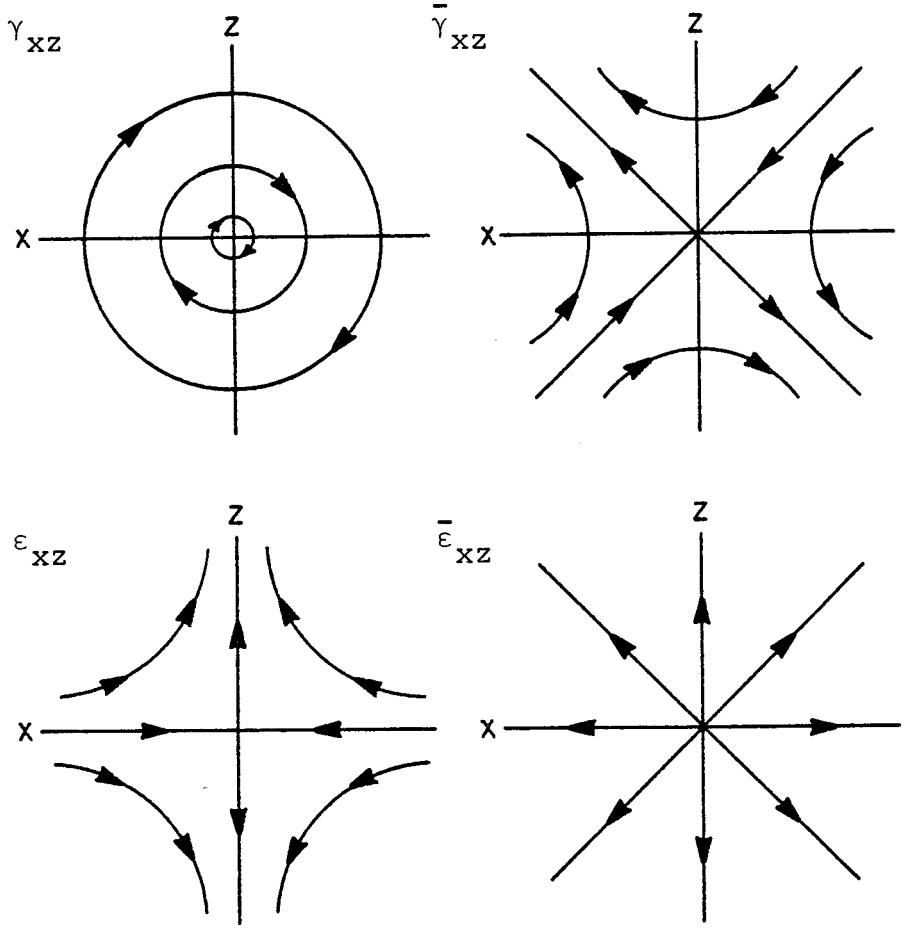

Figure 2.1. Streamlines for in-plane velocity gradient terms.

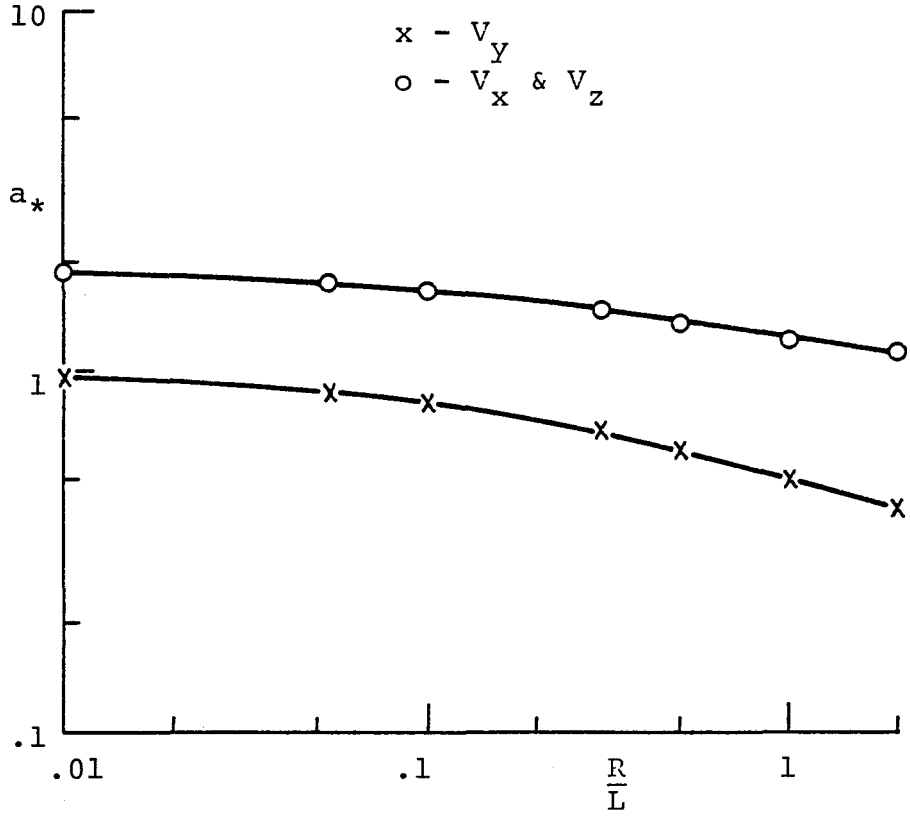

Figure 2.2. Dimensionless parameter a_* for uniform turbulence terms.

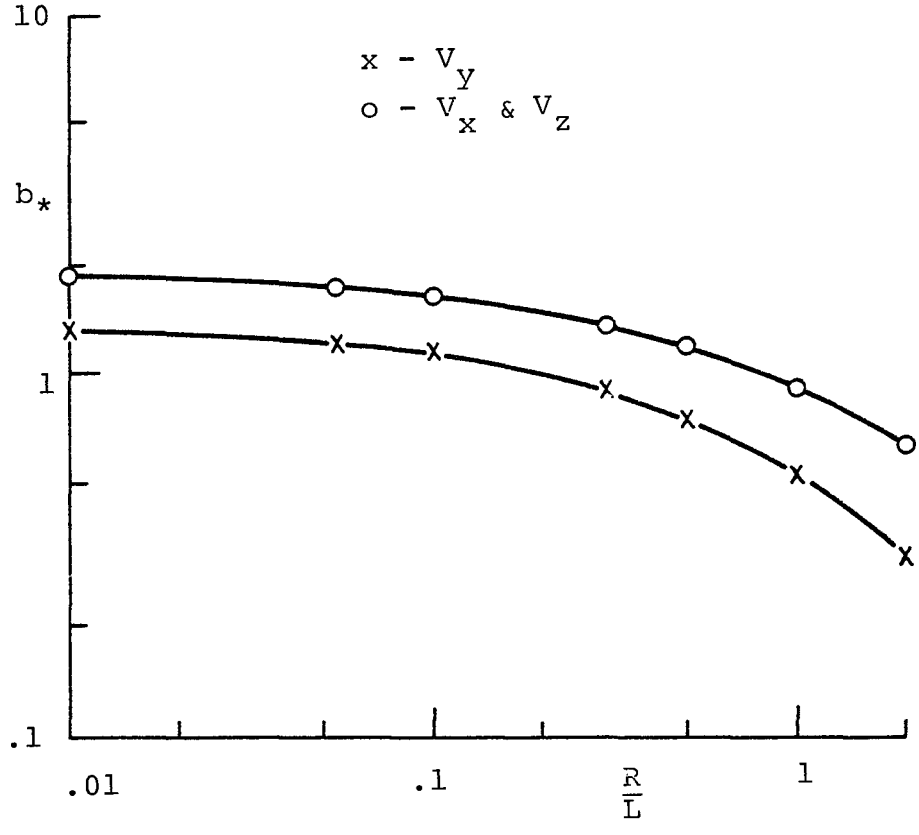

Figure 2.3. Dimensionless parameter b_* for uniform turbulence terms.

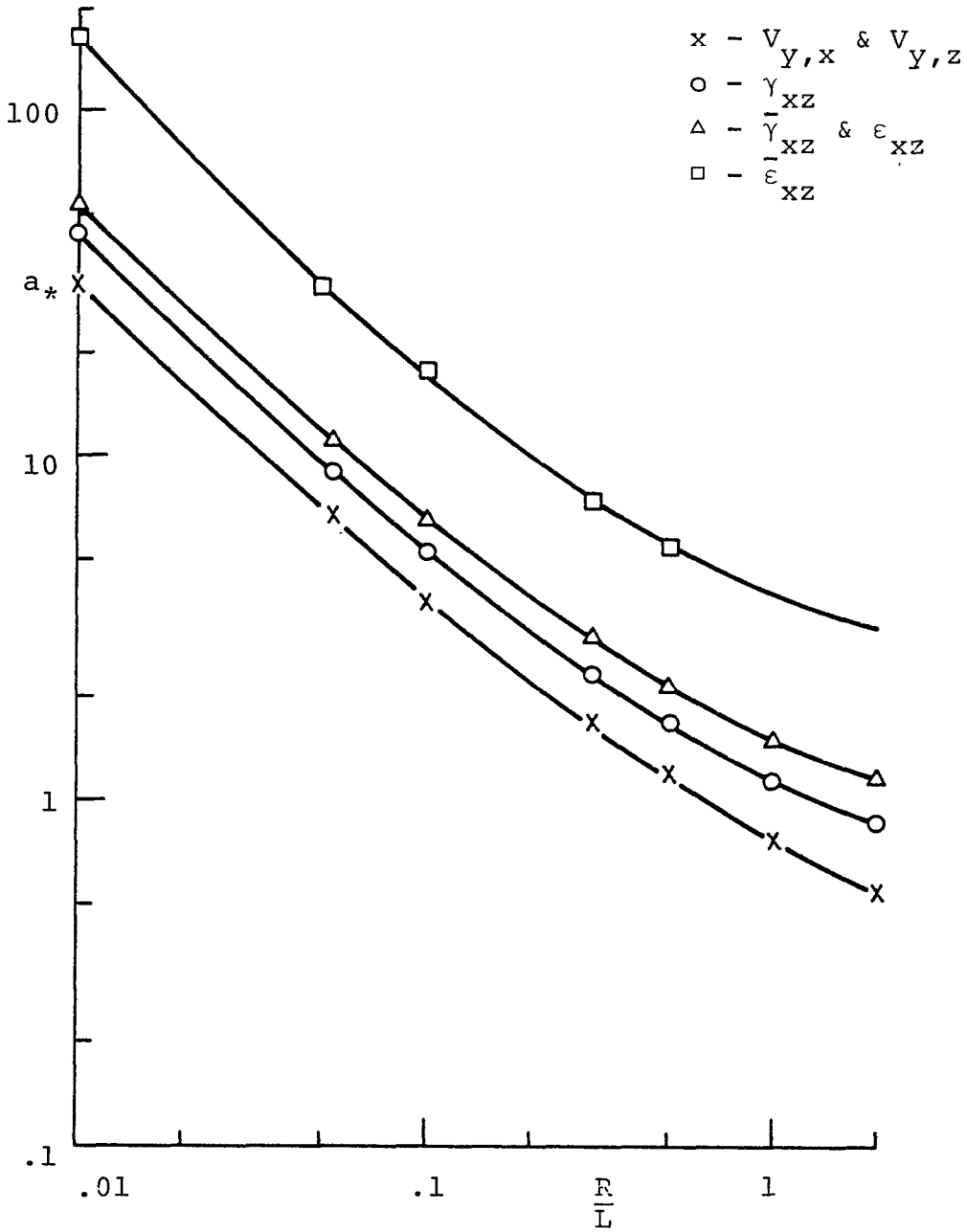

Figure 2.4. Dimensionless parameter a_* for gradient turbulence terms.

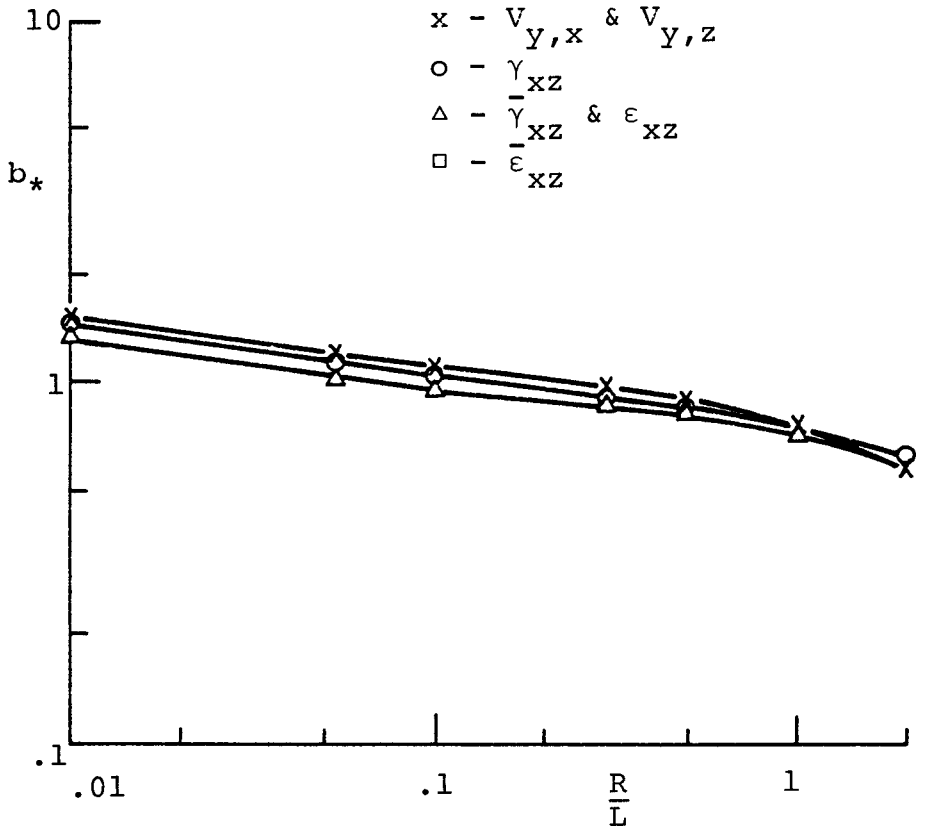

Figure 2.5. Dimensionless parameter b_* for gradient turbulence terms.

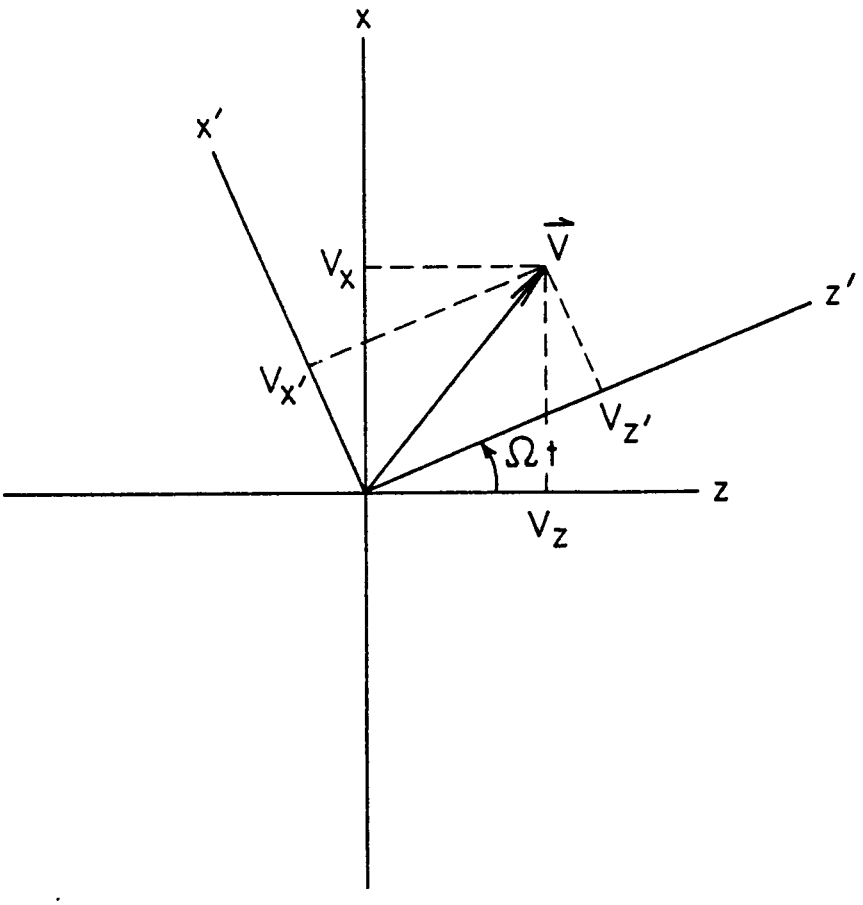

Figure 2.6. Coordinate system for rotating observer.

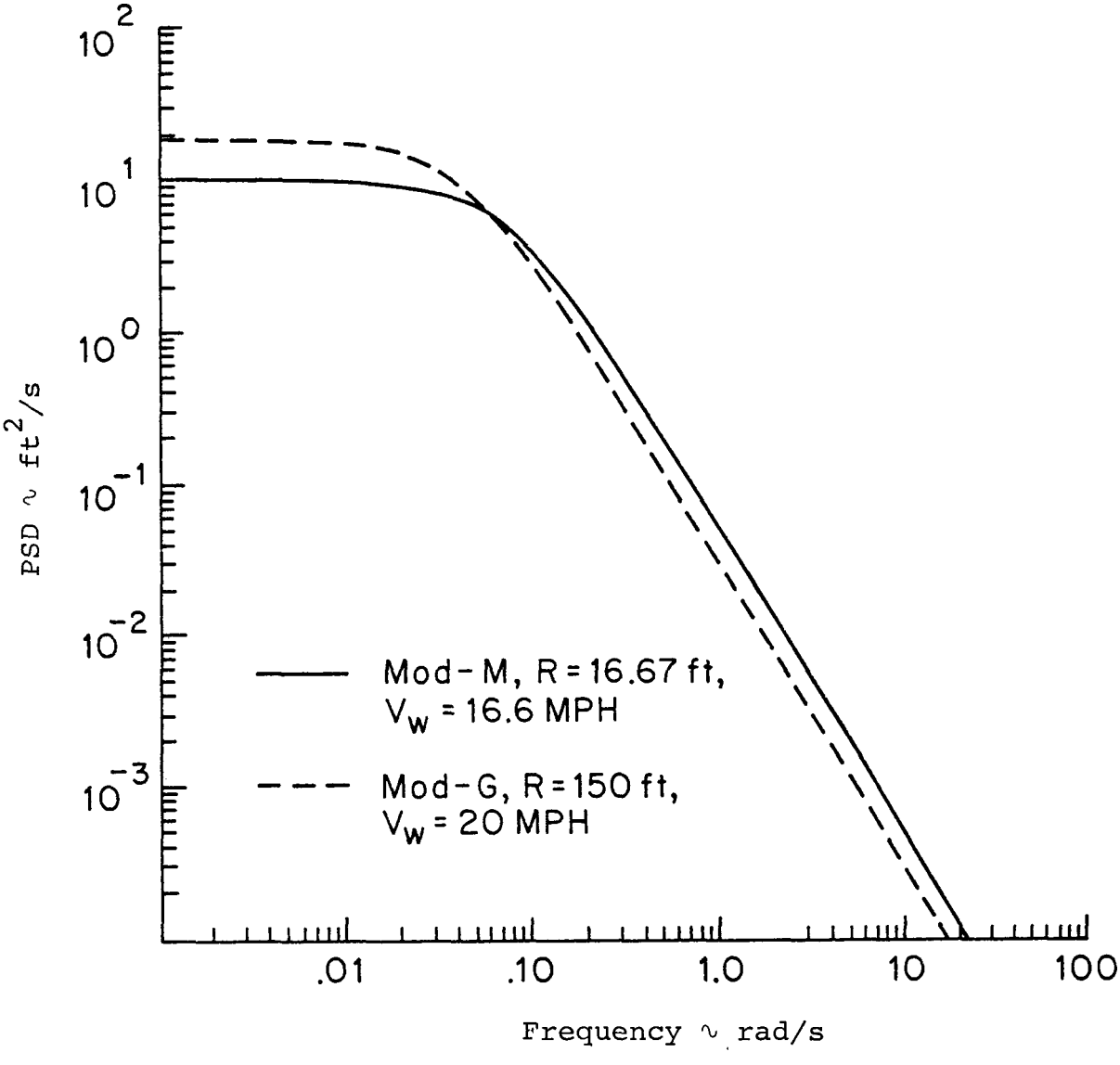

Figure 2.7. Power spectral density for V_y.

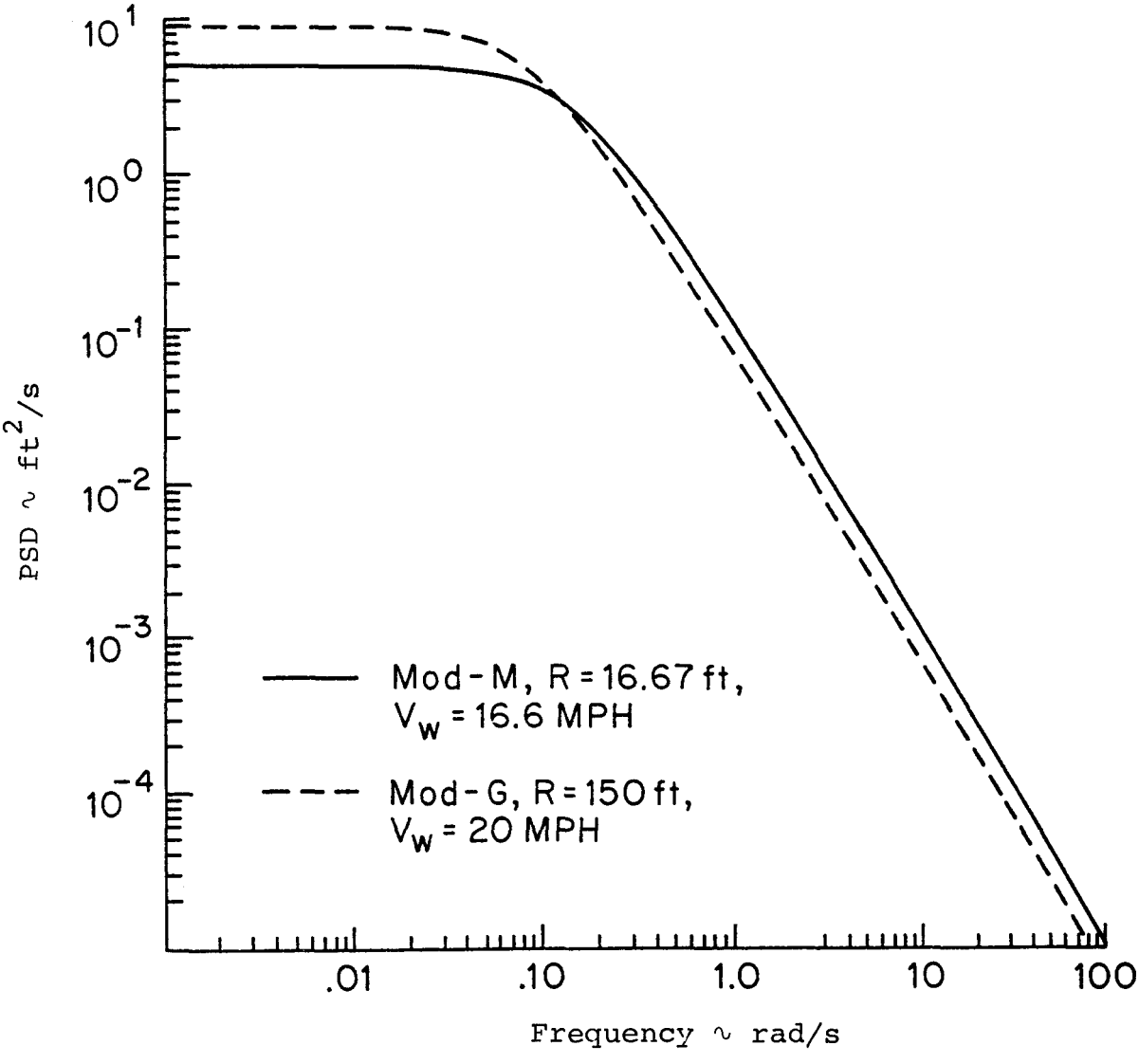

Figure 2.8. Power spectral density for V_x and V_z.

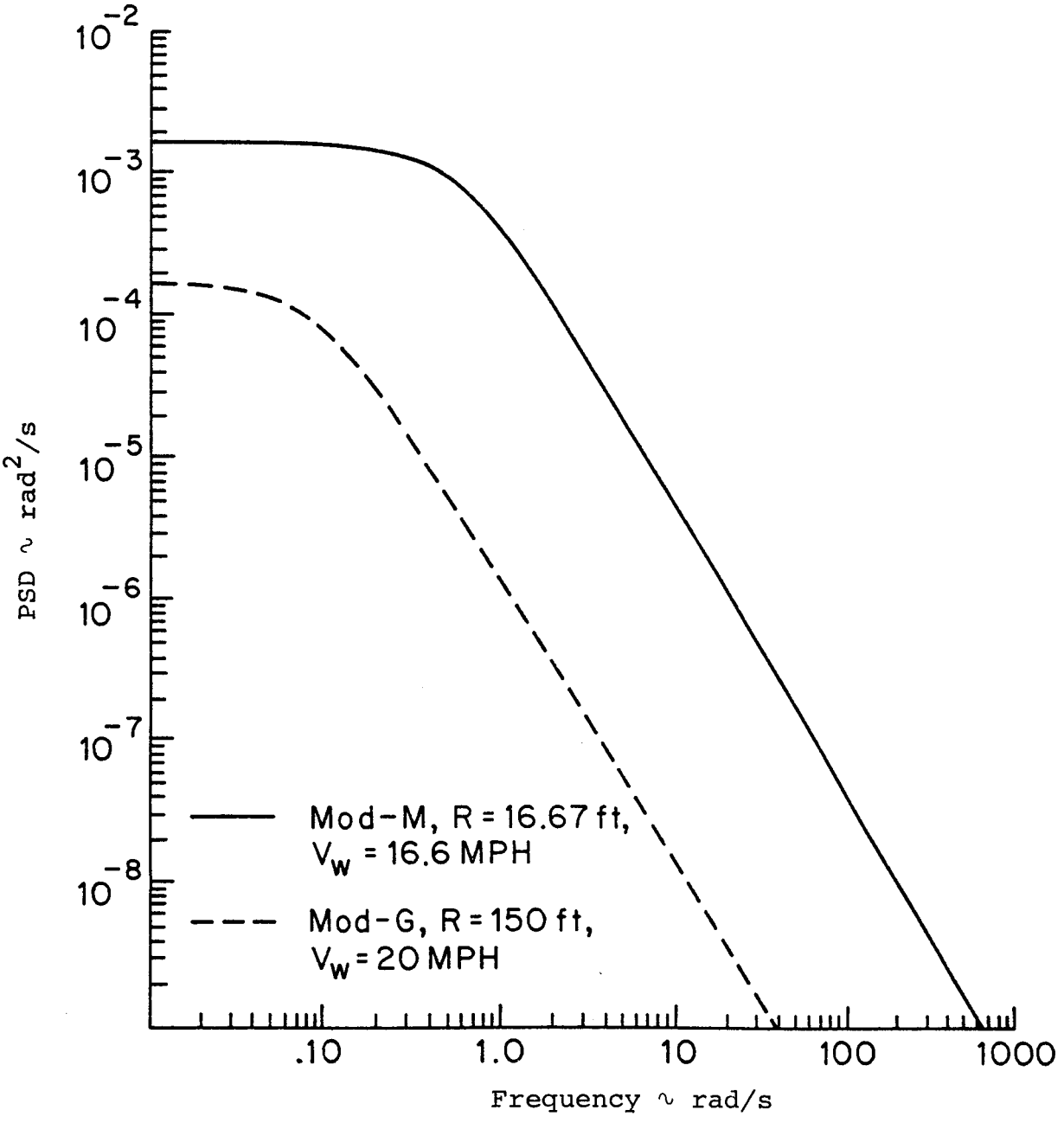

Figure 2.9. Power spectral density for $V_{y,x}$ and $V_{y,z}$.

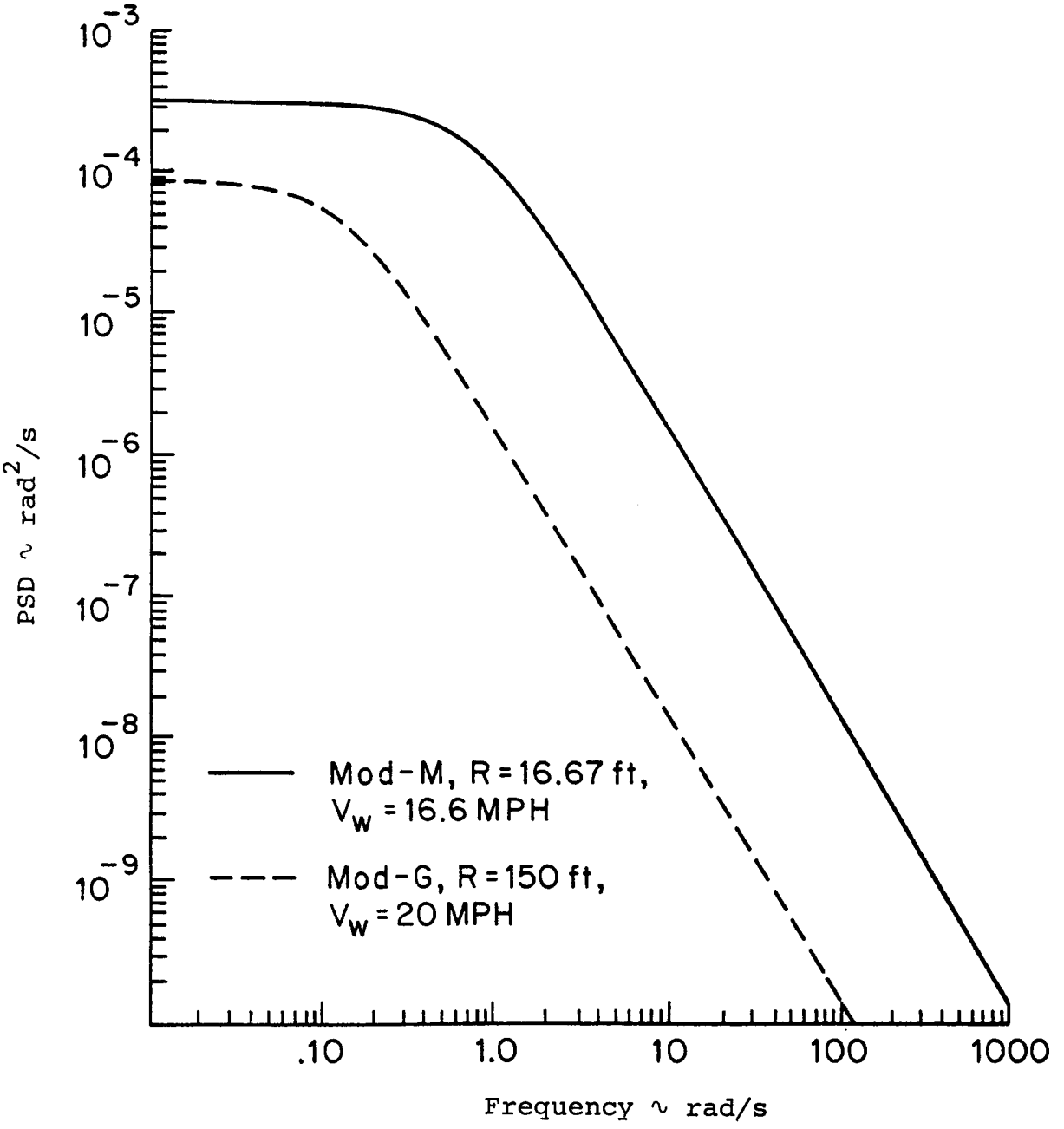

Figure 2.10. Power spectral density for γ_{xz}.

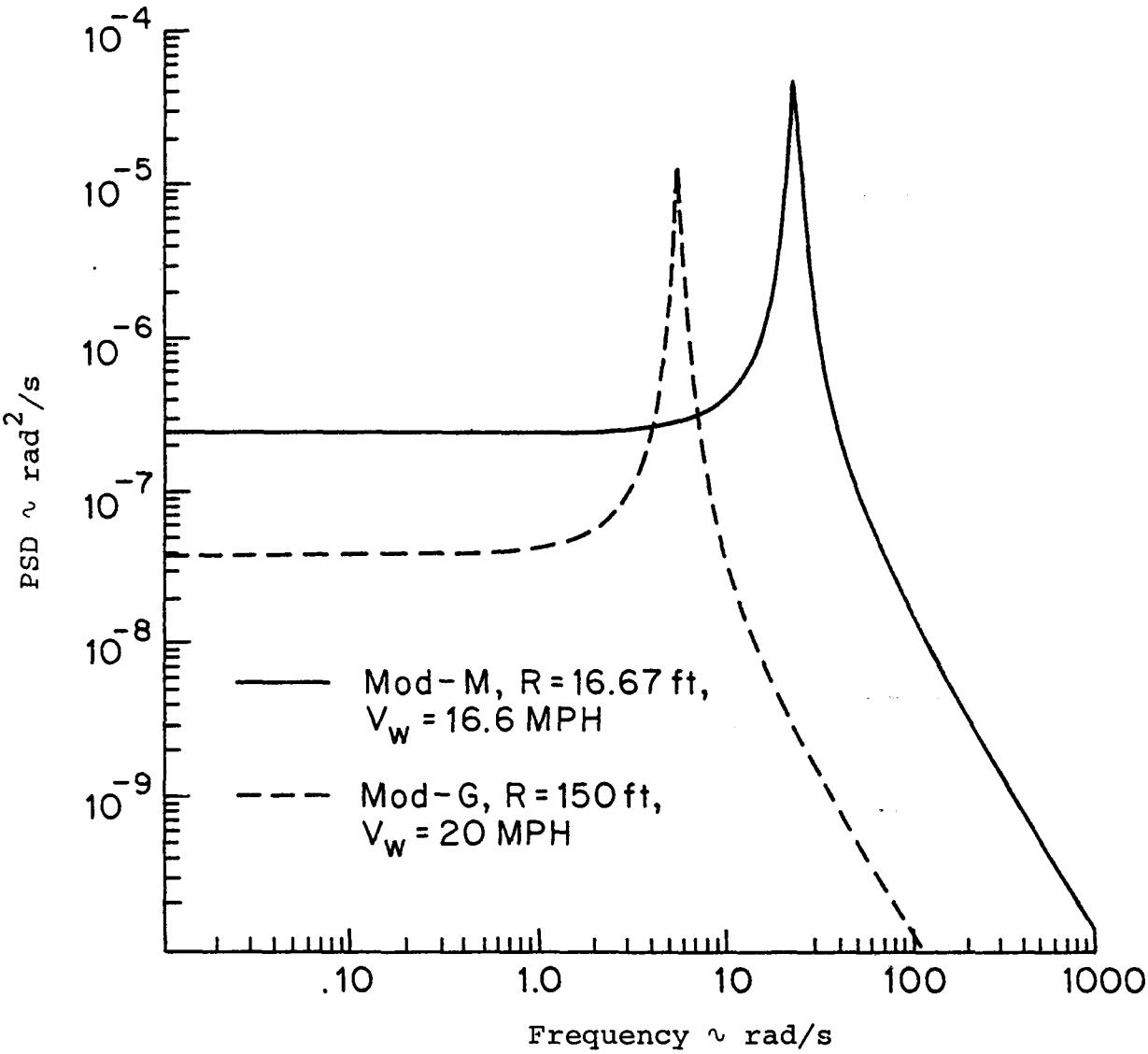

Figure 2.11. Power spectral density for ε_r and $\bar{\gamma}_r$.

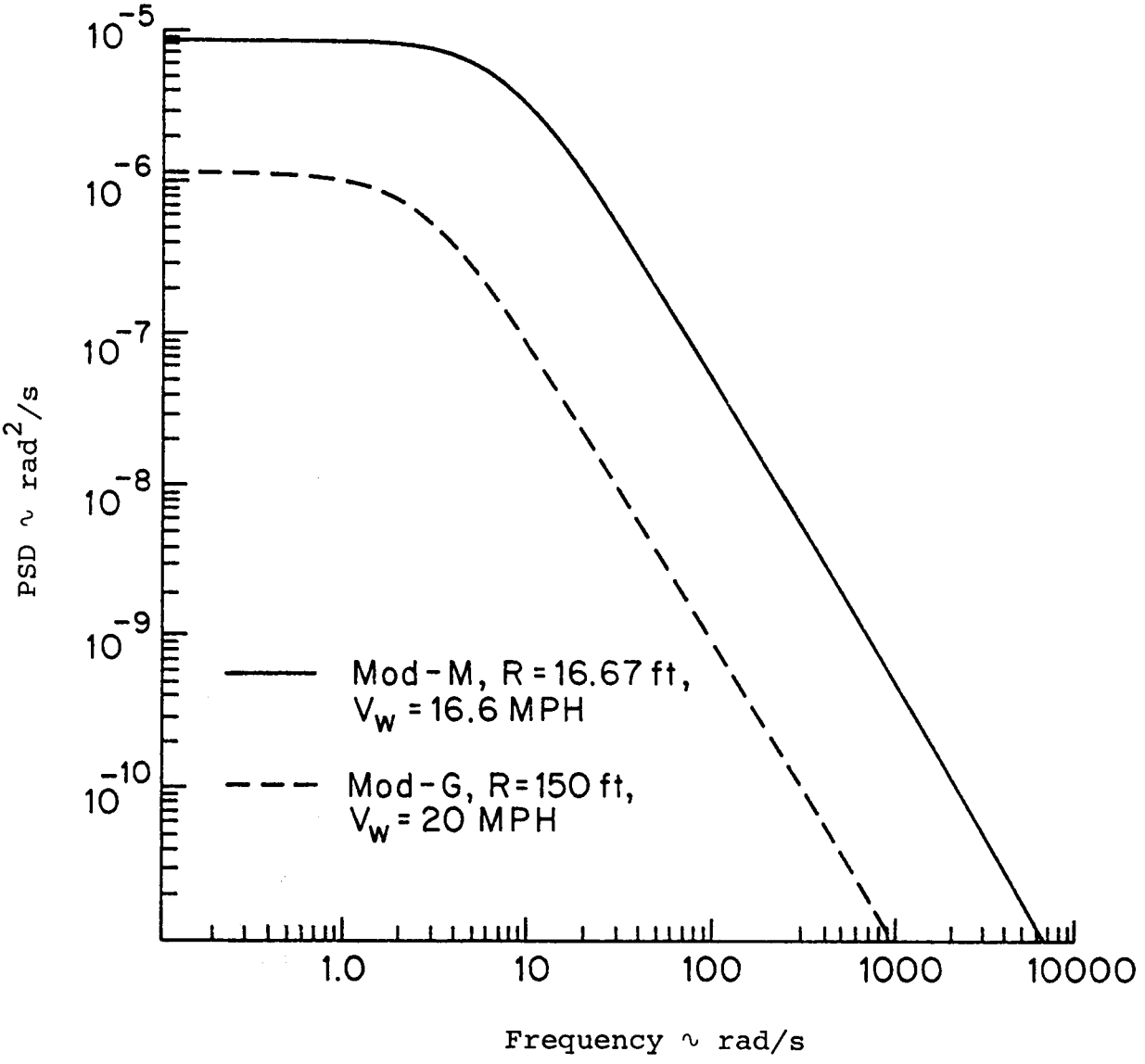

Figure 2.12. Power spectral density for $\bar{\varepsilon}_{xz}$.

CHAPTER 3. THE TURBINE MODEL

3.1 Introduction

It is the objective of this chapter to outline the development of the wind turbine structural and aerodynamic modeling. The structural model involves only a few degrees of freedom, and can only represent lower frequency motions of the system. The emphasis is placed on developing a simple model which can be used to show the sensitivity of wind turbine systems to atmospheric turbulence. The aerodynamic forces are also modeled in a simple manner using the quasi-static strip theory. The idea is to demonstrate the benefit of this type of analysis before progressing to a more complex turbine model. However, in spite of the simple model every effort has been made to retain the key physical responses. A more detailed description of the turbine model is provided in reference 1.

3.2 The Turbine Model

The wind turbine model is shown schematically in Figure 3.1. Both the rotor and the nacelle are assumed to be rigid bodies which move in unison, except for the spinning rotor. Due to tower flexibility, the nacelle and rotor are free to translate in a plane parallel to the ground and rotate about the top of the tower in pitch and yaw. The yaw angle of the rotor axis is defined by the angle, ϕ, and the pitch angle by χ. The lateral translation, U, is in the x direction, while

the V translation is in the y direction along the rotor axis. The rotor spin velocity is given by $\Omega + \dot{\Psi}$, where Ω is the mean rotation rate and $\dot{\Psi}$ is some small fluctuation. For the case of a turbine with a three-bladed rigid rotor, the basic principles of Newtonian mechanics and linear, quasi-steady aerodynamics give motion equations of the form

$$M_{ij}\ddot{X}_j + C_{ij}\dot{X}_j + K_{ij}X_j = F_{ij}U_j \tag{3.1}$$

where M_{ij}, C_{ij}, K_{ij} and F_{ij} are the turbine system inertia, damping, stiffness and wind input coefficients. The five displacement coordinates already described are X_j, while the wind inputs are U_j.

3.3 The Tower

The wind turbine tower is modeled as a single finite element within which the tower displacements are expressed in terms of interpolating polynomials and the displacements at the top of the tower. The tower deformation, v(z,t), about one bending axis is then written in the form

$$v(z,t) = P_V(z)V(t) + P_\chi(x)\chi(t) \tag{3.2}$$

where P_V and P_χ are the interpolating functions which approximate the displacements within the tower. These are conveniently represented as cubic polynomials satisfying the necessary

boundary conditions of a cantilever tower. Using this expression for the tower bending displacement, the stiffness and inertia coefficients may be obtained by one of the numerous energy methods. In terms of the interpolating functions P_V and P_χ, the generalized stiffness and inertia coefficients for the tower may be expressed as

$$k_{ij} = \int_0^L EI(z)P_i''(z)P_j''(z)dz \tag{3.3}$$

$$m_{ij} = \int_0^L m(z)P_i(z)P_j(z)dz \tag{3.4}$$

where EI(z) and m(z) are the stiffness and mass per unit length as a function of height. For additional detail concerning this technique, the interested reader should see Clough and Penzien (2). Although the tower properties are the same in both bending directions, only one degree of freedom is desired for the x direction and therefore rotation of the nacelle about the rotor spin axis is neglected. The method of static condensation is then used to eliminate the unwanted degree of freedom and to obtain the desired x direction stiffness and inertia coefficients as

$$k_{UU} = k_{VV} = k^2_{V\chi}/k_{\chi\chi} \tag{3.5}$$

$$m_{UU} = m_{VV} - 2(k_{V\chi}/k_{\chi\chi})m_{V\chi} + (k_{V\chi}/k_{\chi\chi})^2 m_{\chi\chi} \tag{3.6}$$

In addition, the nacelle and rotor inertias add directly to the tower inertia coefficients, m_{ij}, to give the turbine system inertias. A detailed tabulation of the various terms in the inertia matrix is provided in the Appendix. There is also a gyroscopic coupling between the turbine pitch and yaw motions. This coupling coefficient appears in the damping matrix and is given by

$$C_{\phi\chi} = I_r\Omega = -C_{\chi\phi} \tag{3.7}$$

where I_r is the total effective inertia of all the spinning mass connected to the turbine rotor. Using this simple model the structural stiffness and inertia coefficients for a particular wind turbine are numerically calculated using a TI-59 calculator code (3).

3.4 Aerodynamic Forces

The geometry of the three-bladed rigid rotor is illustrated in Figure 3.2. The blades are coned at an angle β_o, and are assumed to be twisted and tapered. The angle θ defines the pitch setting as the angle from the plane of rotation to the zero-lift-line of the airfoil at the blade tip.

For this analysis, quasi-static aerodynamics will be used to compute the forces acting on the blades due to the turbulent wind and structural motion. The wind input including turbulence is assumed to be made up of a steady mean wind, V_w,

plus fluctuating components, $V_i(t)$, which at any instant are constant over the rotor disk, and turbulence gradients $V_{i,j}(t)$, which vary linearly across the disk. Both $V_i(t)$ and $V_{i,j}(t)$ may be thought as disk averaged time dependent quantities. This allows the wind velocity to be written in a linear expansion as

$$\{V_\infty\} = \begin{Bmatrix} 0 \\ V_w \\ 0 \end{Bmatrix} + \begin{Bmatrix} V_x \\ V_y \\ V_z \end{Bmatrix} + \begin{bmatrix} V_{x,x} & V_{x,y} & V_{x,z} \\ V_{y,x} & V_{y,y} & V_{y,z} \\ V_{z,x} & V_{z,y} & V_{z,z} \end{bmatrix} \begin{Bmatrix} r \sin\Omega t \\ 0 \\ r \cos\Omega t \end{Bmatrix} \tag{3.8}$$

where r is the radial position in the rotor disk, and Ωt is the azimuthal location. Motivation for this particular form for the turbulence is presented in Chapter 2. In this equation the mean wind direction coincides with the y axis of Figure 3.2. In addition, the spatial change in the y direction due to the coning has been dropped in the above expression, which eliminates the effect of the turbulence gradients $V_{i,y}$.

Using the above wind representation and fundamental kinematic relationships, provides the relative velocity as observed from the turbine blade. The relative velocity is made up of contributions from the wind, $\vec{V}_\infty$, the moving structure, $\vec{V}$, and the induced velocity caused by aerodynamic action, $\vec{v}_i$. In equation form this is

$$\vec{V}_{rel} = \vec{V}_\infty - \vec{V} - \vec{v}_i \tag{3.9}$$

In terms of the displacement coordinates, the relative velocity components parallel and perpendicular to the rotor disk rotational plane are given by

$$V_\mu/R\Omega = r\Omega/R\Omega + \{r\dot{\Psi} + \cos\Omega t[-\phi(V_w - v_i) - \delta V_x + \dot{U} - a\dot{\phi}]$$

$$+ \sin\Omega t[-\chi(V_w - v_i) + \delta V_z - a\dot{\chi}]\}/R\Omega$$

$$V_\nu/R\Omega = (V_w - v_i)/R\Omega + \{\delta V_y + \cos\Omega t[-\beta_o \delta V_z + r\dot{\chi}]$$

$$+ \sin\Omega t[\beta_o(\dot{U} - \delta V_x) - r\dot{\phi}]\}/R\Omega \qquad (3.10)$$

where the fluctuating part of the wind turbulence has been written as δV_i to shorten the expressions. These expressions have also been linearized assuming small displacements, and wind fluctuations; however, in some places the product of the static coning angle and the wind fluctuation were retained because of interest in their effect.

Referring to Figure 3.3, the aerodynamic forces parallel and perpendicular to the rotor plane may be written as

$$dA_\mu = \frac{1}{2}\rho a' c\, d\xi\{-\eta V_\mu^2 - \theta V_\nu V_\mu + (1 - \eta/2)V_\nu^2\}$$

$$dA_\nu = \frac{1}{2}\rho a' c\, d\xi\{-\theta V_\mu^2 + (1 + \eta)V_\nu V_\mu - \theta V_\nu^2/2\} \qquad (3.11)$$

where the lift and drag for a blade element have been calculated

using the static formulas with the instantaneous velocities. In the above expressions, a' is the slope of the sectional lift curve $dC_L/d\alpha$, c is the local airfoil chord, η is the ratio C_{D_0}/a' where C_{D_0} is the zero-lift drag coefficient and ρ is the air density.

Using the wind input of Eq. (3.8), together with the velocity expressions of Eq. (3.10) and substituting into the aerodynamic force relationships gives

$$dA_\mu = \frac{1}{2}\rho a' c_t (R\Omega)^2 R dx\{A' - B'[f_o + f_c\cos\Omega t + f_s\sin\Omega t + f_{c2}\cos 2\Omega t + f_{s2}\sin 2\Omega t] + C'[g_o + g_c\cos\Omega t + g_s\sin\Omega t + g_{c2}\cos 2\Omega t + g_{s2}\sin 2\Omega t]\}$$

$$dA_\nu = \frac{1}{2}\rho a' c_t (R\Omega)^2 R dx\{D' + E'[f_o + f_c\cos\Omega t + f_s\sin\Omega t + f_{c2}\cos 2\Omega t + f_{s2}\sin 2\Omega t] + F'[g_o + g_c\cos\Omega t + g_s \sin\Omega t + g_{c2}\cos 2\Omega t + g_{s2}\sin 2\Omega t]\} \qquad (3.12)$$

where the primed quantities are the aerodynamic constants

$$A'(\bar{r}) = [(1 - \eta/2)\lambda^2 - \bar{r}(\eta\bar{r} + \theta\lambda)]c/c_t$$
$$B'(\bar{r}) = [2\eta\bar{r} + \theta\lambda]c/c_t$$
$$C'(\bar{r}) = [(2 - \eta)\lambda - \theta\bar{r}]c/c_t$$
$$D'(\bar{r}) = [(1 + \eta)\lambda\bar{r} - \theta(\bar{r}^2 + \lambda^2/2]c/c_t$$

$$E'(\bar{r}) = [(1 + \eta)\lambda - 2\theta\bar{r}]c/c_t$$
$$F'(\bar{r}) = [(1 + \eta)\bar{r} - \lambda\theta]c/c_t \qquad (3.13)$$

with $\bar{r} = r/R = (h + \xi)/R$, $\lambda = (V_w - v_i)/R\Omega$, and c_t is the chord at the rotor tip. Note that both the pitch setting, θ, and the blade chord, c, may be functions of $\bar{r}$. In the above force equations the subscripted f and g variables are combinations of the wind inputs and response variables and are defined as follows:

$$f_o = r(\dot{\Psi} + \gamma_{zx})/R\Omega$$
$$f_c = -\phi\lambda + (-V_x + \dot{U} - a\dot{\phi})/R\Omega$$
$$f_s = -\chi\lambda + (V_z - a\dot{\chi})/R\Omega$$
$$f_{c2} = -r\,\bar{\gamma}_{zx}/R\Omega$$
$$f_{s2} = r\varepsilon_{zx}/R\Omega$$
$$\gamma_{zx} = \frac{1}{2}(V_{z,x} - V_{x,z})$$
$$\varepsilon_{zx} = \frac{1}{2}(V_{z,z} - V_{x,x})$$
$$g_o = (V_y - \dot{V} - r\beta_o\bar{\varepsilon}_{zx})/R\Omega$$
$$g_c = (r\dot{\chi} + rV_{y,z} - \beta_o V_z)/R\Omega$$
$$g_s = (\beta_o(\dot{U} - V_x) - r\dot{\phi} + rV_{y,x})/R\Omega$$
$$g_{c2} = -\beta_o\, f_{s2}$$
$$g_{s2} = \beta_o\, f_{c2}$$
$$\bar{\gamma}_{zx} = \frac{1}{2}(V_{z,x} + V_{x,z})$$
$$\bar{\varepsilon}_{zx} = \frac{1}{2}(V_{z,z} + V_{x,x}) \qquad (3.14)$$

To obtain the aerodynamic coefficients for the total forces acting on the rotor hub, the appropriate components of the blade

element forces, Eqs. (3.12), are summed over the three blades and integrated with respect to radius for a specified induced velocity distribution. This gives the new thrust, torque, horizontal and vertical forces, and the yaw and pitch moments, which are to be added to the structural terms resulting in the final equations of motion, Eq. (3.1). A detailed list of these equations is provided in the Appendix.

3.5 The Induced Velocity

The aerodynamics of wind turbines involve highly complex flow phenomena, which require rather sophisticated theories in order to obtain accurate predictions. However, some fairly simple theories making relatively crude assumptions can often give reasonable estimates and generally can give excellent insight into the physical phenomena of interest. In this case two different wake models are used in an effort to gain insight into the significance of changes in the induced velocity field on wind turbine response to turbulence.

For the first wake model, the induced velocity is computed using blade element theory following the approach of Wilson (4), and performing a momentum balance neglecting wake rotation. This provides the induced velocity as a function of radius, under the assumption that the rotor axis is perfectly aligned with the wind direction. After the induced velocity distribution is computed for a given mean operating condition, it is assumed to be constant and independent of turbulent wind fluctuations.

This model is named the "frozen wake."

The second wake model is called the "equilibrium wake." For this model, the axial fluctuations in wind velocity are assumed to occur so slowly that the induced velocity is the steady state value for the instantaneous wind speed. In this situation, the axial flow will not only be time varying but also will be nonuniform, because of the inclusion of the fluctuating wind gradient terms in the turbulence model of Eq. (3.8). These gradients could be thought of as slowly changing wind shears of arbitrary orientation, since their effect on the wind turbine is similar. To obtain an approximation for the induced velocities of this "equilibrium wake," the "semi-rigid" wake model discussed by Miller (5) is used. Miller shows that the effect of including the induced velocity due to the nonuniform flow is to reduce the lift by a factor referred to as the "lift deficiency" function.

For this analysis, assuming small velocity changes, the lift deficiency function is approximately

$$\mathcal{L}_d(\bar{r}) = \frac{1}{1 + \tau_t F'(\bar{r})/\bar{r}(2\lambda - \lambda_w)} \tag{3.15}$$

where $\lambda_w = V_w/R\Omega$ and $\tau_t = 3a'c_t/8\pi R$. In addition, the azimuthal change in the induced velocity distribution leads to a change in the in-plane aerodynamic coefficients $B'(\bar{r})$. This change is given by

$$\Delta B'(\bar{r}) = \tau_t [B'(\bar{r})F'(\bar{r}) + C'(\bar{r})E'(\bar{r})]/\{\bar{r}(2\lambda - \lambda_w)\} \qquad (3.16)$$

Because this change is small, it is tempting to neglect it. However, all of the in-plane forces are small so it will be retained. Finally, the wind fluctuations in the axial direction V_y, $V_{y,z}$ and $V_{y,x}$ are associated with a change in momentum in the streamwise direction which, for the assumptions of this wake model, change the equilibrium thrust. This added lift factor is approximately

$$\mathcal{K}_a(\bar{r}) = 1 + \lambda/(2\lambda - \lambda_w) \qquad (3.17)$$

To incorporate these effects, the aerodynamic coefficients $B'(\bar{r})$, $C'(\bar{r})$, $E'(\bar{r})$ and $F'(\bar{r})$ of Eqs. (3.13) are modified in the following manner to obtain the "equilibrium wake" coefficients:

$$\begin{aligned}
B'_e(\bar{r}) &= \mathcal{K}_d(\bar{r})\{B'(\bar{r}) + \Delta B'(\bar{r})\} \\
C'_e(\bar{r}) &= \mathcal{K}_d(\bar{r})C'(\bar{r}) \\
E'_e(\bar{r}) &= \mathcal{K}_d(\bar{r})E'(\bar{r}) \\
F'_e(\bar{r}) &= \mathcal{K}_d(\bar{r})E'(\bar{r}) \\
C'_{ey}(\bar{r}) &= \mathcal{K}_d(\bar{r})\mathcal{K}_a(\bar{r})C'(\bar{r}) \\
F'_{ey}(\bar{r}) &= \mathcal{K}_d(\bar{r})\mathcal{K}_a(\bar{r})C'(\bar{r})
\end{aligned} \qquad (3.18)$$

where the two coefficients C'_{ey} and F'_{ey} are specifically associated with the wind fluctuations V_y, $V_{y,z}$ and $V_{y,x}$. The aerodynamic coefficients $A'(\bar{r})$ and $D'(\bar{r})$ are related to the mean

thrust and torque and are thus unaffected by wind fluctuations. Computationally, the influence of the wake model can be observed by replacing the primed aerodynamic coefficients of Eqs. (3.13) with those of Eqs. (3.18) above.

Although both of these wake models are useful in developing an understanding of the influence of the induced velocity distribution on machine response to turbulence, it is unclear whether either model accurately approximates the real distributions and future work is needed to evaluate the effects of unsteady wake aerodynamics.

3.6 State Space Equations

The equations of motion Eq. (3.1) can be written in matrix form

$$[M]\{\ddot{X}\} + [C]\{\dot{X}\} + [K]\{X\} = \{Q_1\} + [F]\{u\} \tag{3.19}$$

where

$\{X\}^T = (U,V,\phi,\chi,\Psi)$ = displacement coordinate

$\{Q_1\}^T = (0,T,0,Q,0)$ = steady state

$\{u\}^T = (V_x,V_y,V_z,V_{y,x},V_{y,z},\gamma_{xz},\varepsilon_r,\bar{\gamma}_r,\bar{\varepsilon}_{xz})$ = wind inputs

$\varepsilon_r = \varepsilon_{zx}\cos 3\Omega t + \bar{\gamma}_{zx}\sin 3\Omega t$

$\bar{\gamma}_r = -\varepsilon_{zx}\sin 3\Omega t + \bar{\gamma}_{zx}\cos 3\Omega t$

The terms ε_r and $\bar{\gamma}_r$ come from the three-bladed sums of the terms f_{c2}, f_{s2}, g_{c2}, and g_{s2} in Eqs. (3.14). They can be interpreted as components of a vector which rotates at three times the rotor rate.

It is possible to model each of the nine turbulence

inputs using a set of stochastic differential equations of the form

$$\{\dot{u}\} = [A_w]\{u\} + [B_w]\{w\} \tag{3.20}$$

where the components of $\{w\}$ are white noise of equal power spectral density, $[B_w]$ is the white noise input distribution matrix which is diagonal. The $[A_w]$ matrix is diagonal except for two elements

$$[A_w] = \begin{bmatrix} a_{11} & & & \\ & \ddots & & \\ & & a_{77} & 3\Omega \\ & & -3\Omega & a_{88} \\ & & & & a_{99} \end{bmatrix}$$

which arise as a result of the $\sin 3\Omega t$ and $\cos 3\Omega t$ in the ε_r and $\bar{\gamma}_r$ wind inputs. The source of these two off diagonal terms 3Ω and -3Ω is described in more detail in Chapter 2.

Discarding the steady terms, it is convenient to transform the equations of motion given in Eq. (3.19) to the state space form, so that they are written as a set of first order equations similar to the turbulence inputs of Eq. (3.20). To further facilitate the computation of results, the state space form of Eq. (3.19) can be augmented with the turbulence inputs,

Eq. (3.20), to form a single system of equations with white noise as the driving input. The five turbine displacements and their derivatives together with the nine turbulence inputs will form the state vector for this augmented system. The governing equations can then be written

$$\{\dot{x}\} = [A]\{x\} + [B]\{w\}$$

$$\{y\} = [c]\{x\} \tag{3.21}$$

where

$$\{x\} = \begin{Bmatrix} X \\ \{\dot{X}\} \\ \{u\} \end{Bmatrix} \qquad [A] = \begin{bmatrix} [0] & [I] & [0] \\ -[M]^{-1}[K] & -[M]^{-1}[K] & [M]^{-1}[F] \\ [0] & [0] & [A_w] \end{bmatrix}$$

$$[B] = \begin{bmatrix} [0] \\ [B_w] \end{bmatrix} \qquad \{y\} = \begin{Bmatrix} F_x \\ F_y \\ M_z \\ M_x \\ \text{Power} \\ \{x\} \end{Bmatrix} = \text{outputs}$$

$$[c] = \begin{bmatrix} [K] & [0] \\ (00\ldots\Omega c_g\ldots 0) & \\ [I] & \end{bmatrix} = \text{response matrix}$$

With this formulation it is a relatively straightforward numerical procedure, to determine the complex eigenvalues of the A matrix and then to compute the modal matrix, which is made up of the associated eigenvectors. The modal matrix can then be used to decouple the equations of motion so that transfer functions between any of the nine white noise inputs and any output, y_i, may be easily computed. These transfer functions account for differences in the energy level for the turbulence inputs, {u}, so that a comparison of the transfer function magnitudes provides a direct estimate of relative importance. The final result uses the central equation from random vibration theory (6), which states that the spectral density for any of the outputs {y} will be given by

$$\{S_y(\omega)\} = [|H_{yw}(\omega)|^2] \{S_w\} \tag{3.22}$$

for uncorrelated inputs. In this equation, $\{S_y(\omega)\}$ is the spectral density of the outputs {y}, $[|H_{yw}(\omega)|^2]$ is the matrix consisting of elements which are the square of the transfer function magnitude and $\{S_w\}$ is the flat spectral density of the white noise driving inputs, which are all equal.

3.7 References

1. Thresher, R.W., et al., Modeling the Response of Wind Turbines to Atmospheric Turbulence, Oregon State University Report RL0/2227-80/2, 1981.

2. Clough, R.W. and Penzien, J., Dynamics of Structures, McGraw-Hill, 1975.

3. Jafarey, N., and Thresher, R., "Turbine System Natural Frequencies," Program Record for TI-59 Programmable Calculator, Program Records No. 101 and 102, Mech. Engrng. Dept., Oregon State University.

4. Wilson, R.E., and Lissaman, P.B.S., Applied Aerodynamics of Wind Power Machines, Oregon State University Report, NTIS PB-238-595, 1974.

5. Miller, R., Dugundji, J., Martinez-Sanchez, M., Gohard, J., Chung, S., and Humes, T., Aerodynamics of Horizontal Axis Wind Turbines, Volume II of Wind Energy Conversion, Report ASRL TR-184-8, Dept. of Aeronautics and Astronautics, MIT, Sept. 1978.

6. Newland, D.E., An Introduction to Random Vibration and Spectral Analysis, Longman, 1975.

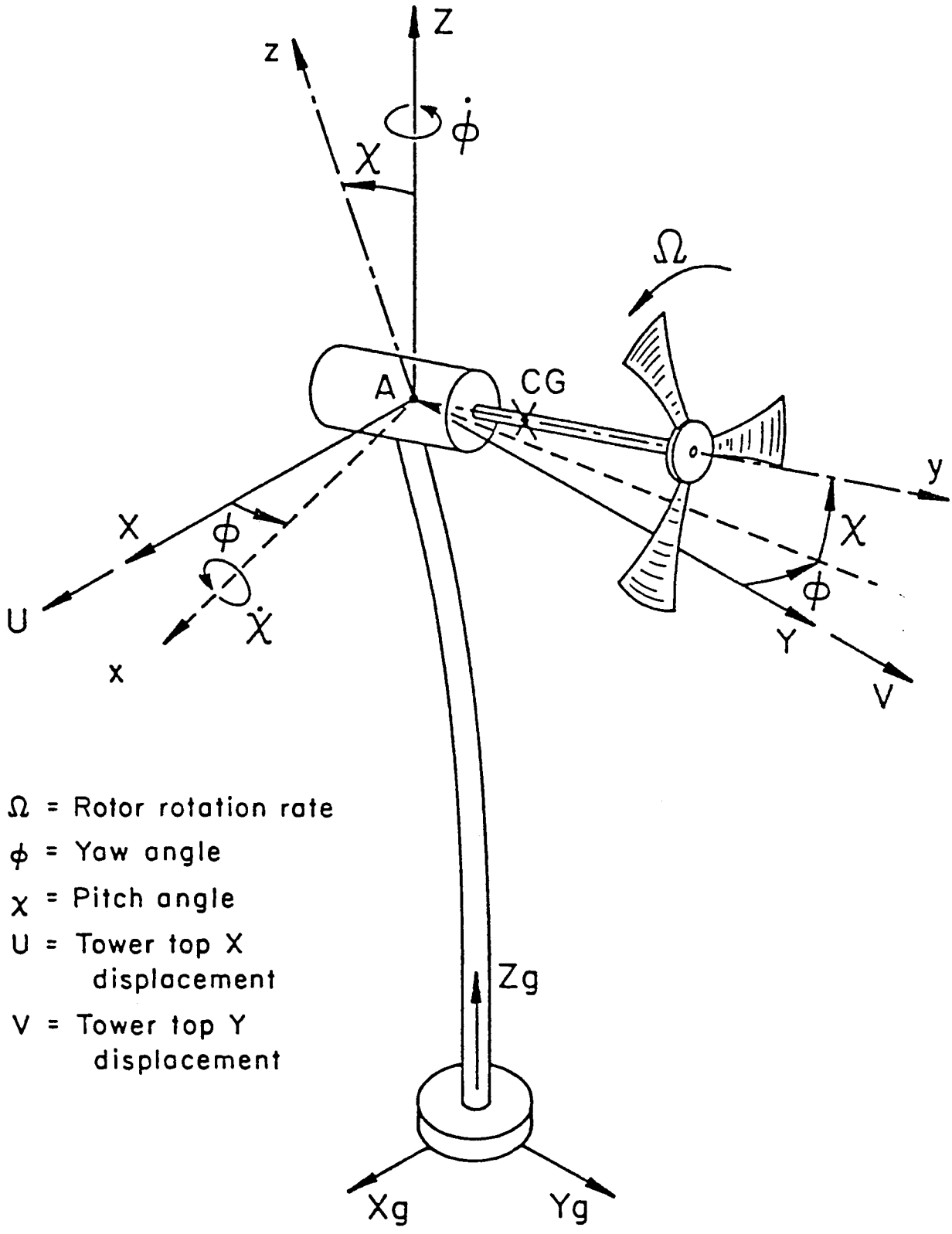

Figure 3.1. The Turbine Model

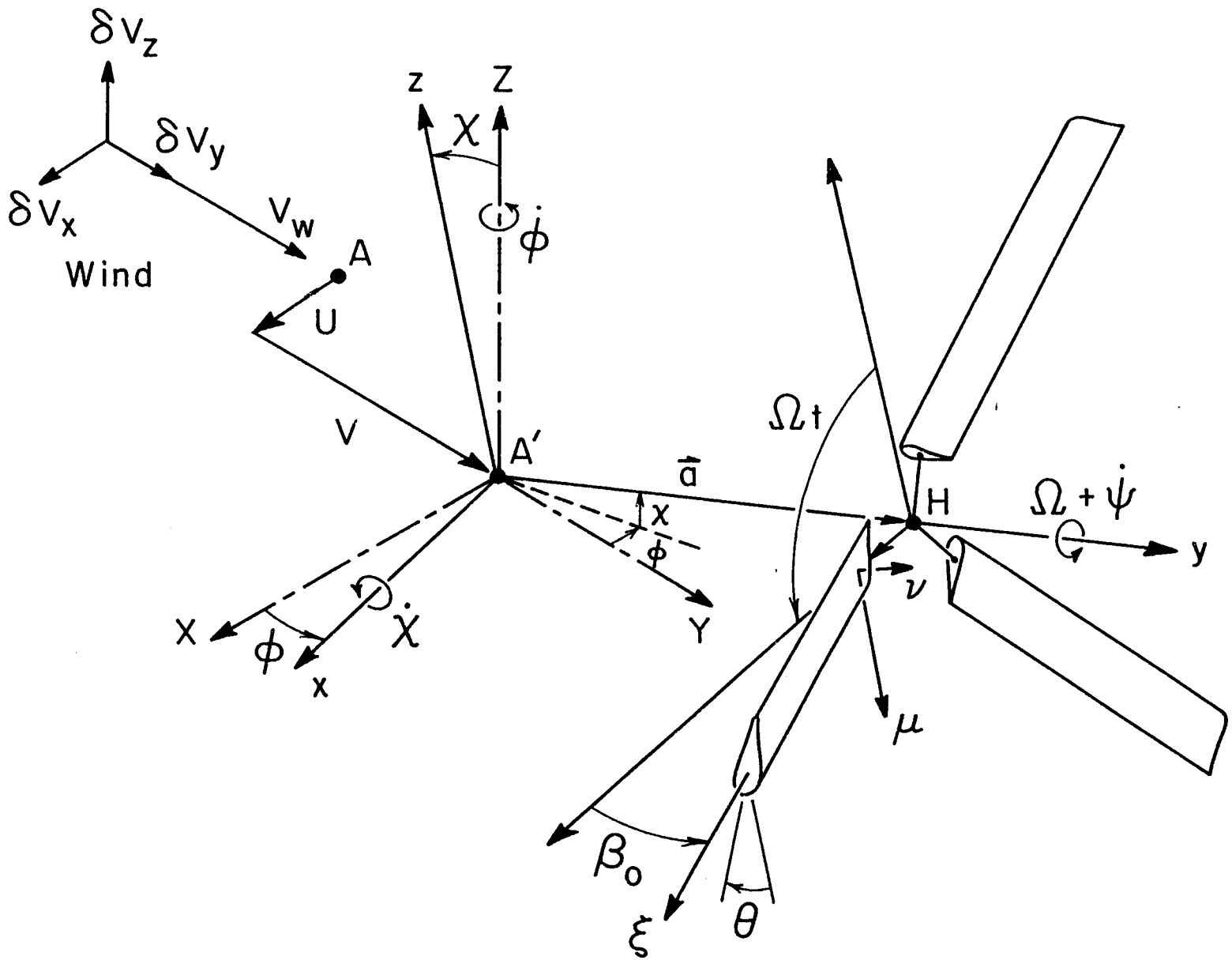

Figure 3.2. Rotor Geometry

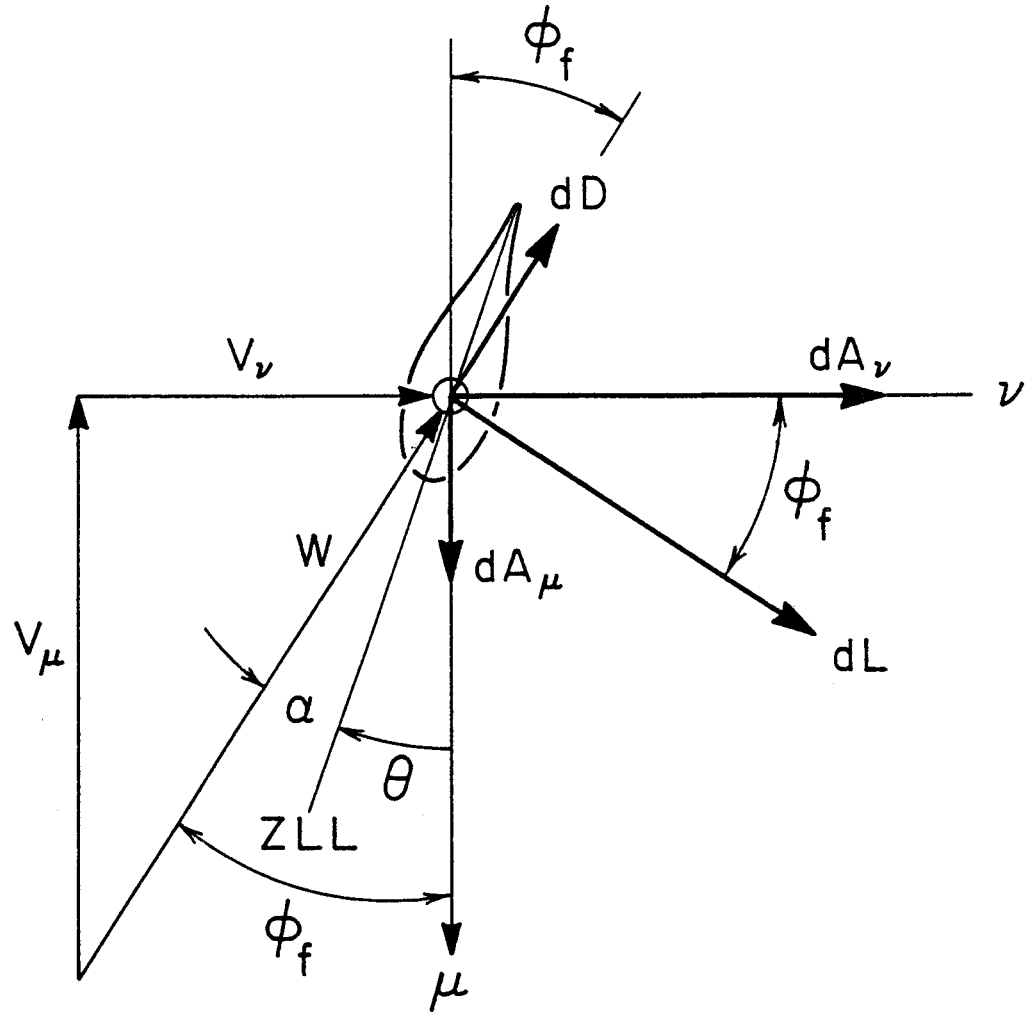

Figure 3.3. Blade Element Aerodynamic Forces

CHAPTER 4. MODELING RESULTS

4.1 Introduction

This chapter presents results for two wind turbine systems of vastly different sizes based on the models explained in the previous two chapters. In keeping with the form of the DOE nomenclature, the smaller 8 kW machine is designated the Mod-M in this report. This nomenclature evolved from the nickname "Mini-Mod" which was used while the model was being developed. This machines is typical of the small machines that are tested at the Rocky Flats Test Site. In contrast to this small system, a large wind turbine, designated the Mod-G, was modeled. The "G" designation arose from the gigantic 300 ft diameter and 2.5 MW nominal power. This machine is similar in size to the DOE Mod-2 wind turbine. The primary objective of this chapter is to examine the response of these two turbines using the methods outlined in the previous chapters, and to determine the sensitivity of these systems to atmospheric turbulence.

4.2 Response of a Small Turbine

The small, Mod-M, is an 8 kW system, with three blades located downwind of the tower and designed for free-yaw operation. The specific machine characteristics are shown in Table 4.1. With the structural characteristics for this system as outlined in the Appendix, and the atmospheric turbulence parameters for the wind inputs as specified in

Table 4.1. Mod-M Characteristics

Rotor Characteristics (Rigid Rotor):			
Rotor Radius		16.67	ft
Blade Chord (constant)		1.5	ft
Coning Angle		3.5°	
Blade Twist		0.0°	
System Frequencies (Tower Motions):			
1st Bending (fore-aft)	(2.0Ω)	15.5	rad/s
2nd Bending (fore-aft)	(7.0Ω)	53.5	rad/s
1st Torsion	(Free yaw)	0.0	rad/s
1st Bending (side-to-side)	(2.1Ω)	15.9	rad/s
Aerodynamic Properties:			
Lift Curve Slope		5.7	
Drag Coefficient, C_{D_0}		.02	
Stall not modeled			
Operating Conditions Used:			
Wind Velocity (mean)		16.63	MPH
Rotor Speed (mean)	(7.81 rad/s)	73.35	RPM
Pitch Setting (to ZLL)		3.0°	
Turbulence Length Scale		300	ft
Rms Turbulent Intensity		2.03	ft/s
Approximate Output		6	kW

Table 2.3, the dynamic response is computed using the approach outlined in Section 3.6. The most revealing response variables are the yaw angle and the forces and moment which act at the top of the tower. These response variables are shown in the power spectral density plots of Figures 4.1 through 4.4. In these figures the system resonances are identified and the difference in response for each of the two wake models is illustrated. The somewhat larger response predicted by the equilibrium wake is associated with the change in momentum in the streamwise direction, which for the equilibrium wake model results in additional lift. The major feature of Figure 4.1 is the significant response at the system side-to-side bending frequency. Figure 4.2 shows similar responses at the two system fore-aft bending frequencies. In Figure 4.3, the marked decrease in yaw response above 0.1 rad/s (.016 hz) is noticeable, which implies that this free-yaw turbine only follows the low frequency wind disturbances. Figure 4.4 gives the tower pitching moment response and shows the same type of resonance peaks as the other figures. For the equilibrium wake, the increase in pitching moment between .1 to 1 rad/s seems to be associated with the decrease in yaw response, and illustrates the coupling between turbine pitch and yaw motions, even for a free-yaw system. Figure 4.4 also shows a small response peak at 3Ω, which is the result of the $\sin 3\Omega t$ and $\cos 3\Omega t$ in the ε_r and $\bar{\gamma}_r$ inputs.

4.3 Response of a Large Turbine

The second wind system to be analyzed in this study is a large turbine called the Mod-G. The Mod-G is a 2.5 MW turbine with a three-bladed rotor located upwind of the tower, and is designed for fixed-yaw operation. The specific characteristics of this system are shown in Table 4.2. Figures 4.5 through 4.8 present the computation results for the Mod-G turbine, with the exception that since this is a controlled yaw machine, yaw moment response rather than yaw angle response is plotted. The general pattern of results is quite similar to the Mod-M with the resonances marked by characteristic spikes. If it were desired to build one of these turbines, the details of these curves would be very useful. The interest here, however, is in determining the sensitivity of these two systems to the turbulence inputs.

4.4 Power Output

The equations of motion in the Appendix show that the only coupling between the generator and the rest of the system is through the single damping coefficient C_{52}. If this coefficient were zero, the drive train response would be independent of the other structural motions. For the systems considered in this report, this coupling is weak, and for all practical purposes, one can consider the power train independent of the rest of the system. However, it should be remembered that a direct path for coupling the generator output to structural

Table 4.2. Mod-G Characteristics

Rotor Characteristics:			
Rotor Radius		150	ft
Blade Chord (linear taper)		7.74 ft at hub to 3.15 ft at tip	
Coning Angle		4°	
Blade Twist (linear)		8°	
System Frequencies:			
1st Bending (fore-aft)	(1.5Ω)	2.7	rad/s
2nd Bending (fore-aft)	(7.5Ω)	13.7	rad/s
1st Bending (side-to-side)	(1.6Ω)	2.9	rad/s
1st Torsion	(4.9Ω)	9.0	rad/s
Aerodynamic Properties:			
Lift Curve Slope		5.73	
Drag Coefficient, C_{D_0}		.008	
Stall not Modeled			
Operating Conditions:			
Wind Velocity	(1.833 rad/s)	20	MPH
Rotor Speed		17.5	RPM
Pitch Setting at Tip		-6.2°	
Turbulence Length Scale		500	ft
Rms turbulent intensity		2.44	ft/s
Approximate Power Output		1.1	MW

motion was eliminated from the model, when the tower rotational degree-of-freedom about the rotor spin axis was removed. This was described in Section 3.3. Without this degree of freedom, the generator torque acting on the top of the tower is assumed to be negligible. In addition, this prevents roll motion of the nacelle which would realistically influence the relative velocity of the rotor with respect to the wind. One can, therefore, come to no firm conclusions concerning the degree of coupling between the tower motion and power output, because the model, due to its simplicity, has prevented these interactions. Supporting this simplified model is the fact that field test data has not yet uncovered any significant coupling between the drive train and the tower, and it is standard practice to treat the wind turbine drive train as if it were completely independent of the tower structure. The reader should see Sullivan, Miller and Spera (1) and Martinez-Sanchez (2) for more details on these drive train models.

Two different models are used for the generator and drive train. In the first, it is assumed that power fluctuations about the mean power are a linear function of the rotor speed fluctuations about the mean. This gives the power output as

$$P = (\Omega C_g \dot{\Psi}) \eta_e \tag{4.1}$$

where C_g is the generator torque coefficient, Ω is the mean rotor speed, $\dot{\Psi}$ is the fluctuation in rotor speed, and η_e is

the overall power conversion efficiency. This is mechanically equivalent to having a viscous dissipator connected directly to the rotor. This model eliminates any possibility of a drive train resonance, and treats the generator as if it were a viscous power element.

The second model assumes that the drive train is an elastic spring and that the generator on the output shaft always rotates at constant speed, Ω, while the rotor on the other end is free to respond to wind fluctuations. This will give the output power as

$$P = \Omega(k_g \Psi)\eta_e \tag{4.2}$$

where k_g is the drive train spring rate. Although, neither of these models is really correct, they will provide bounds on the behavior which can be expected. In an elementary sense, the first model responds like an induction generator, while the second has characteristics like a synchronous generator. Better models would require additional degrees of freedom.

Figures 4.9 through 4.12 show the results for both power train models on the Mod-M and the Mod-G using both wake models. For the Mod-M the drive train spring rate was set so that the natural frequency was approximately 1.4Ω, and for the Mod-G, it was set at $.5\Omega$. The results for the elastic drive train show the characteristically large spikes at the drive train natural frequency, and those for the viscous power element

show almost no response except for a small downward spike at the first tower natural frequency, where the tower motion removes energy which would normally go to the generator. This was the only observed coupling between the drive train and other structural motions.

4.5 The Key Turbulence Inputs

The primary objective of this work was to identify the features of turbulence which are most important in wind turbine design. In an effort to focus on these key features, the response at specific system frequencies was broken down into fractional contributions from each turbulence input. The most significant results of these calculations are tabulated in Tables 4.3 and 4.4.

From these results it seems clear that the most important inputs are the longitudinal turbulence component, V_y, the two associated gradient terms $v_{y,x}$ and $v_{y,z}$, and the two in-plane turbulence terms $\bar{\gamma}_r$ and ε_r which have an effective frequency of 3Ω.

To examine this conclusion more closely, consider Figures 4.13 through 4.18, which present plots of power spectral densities for the various response variables using, first, only the turbulence input V_y, and then comparing it with the results when the two gradients $V_{y,x}$ and $V_{y,z}$ are added to the input. Figures 4.13 and 4.17 show that when computing thrust, the second mode bending response is virtually eliminated unless these two gradient terms are included. However, this deficiency is minor

Table 4.3. Fractional Response Contributions of the Turbulence Inputs for the Mod-M Using the Equilibrium Wake

Response/Input	V_y	$V_{y,x}$	$V_{y,z}$	ε_r	$\bar{\gamma}_r$	Other
Frequency ≈ 0						
Side Force, F_x	.0	.96	.0	.0	.0	.04
Thrust, F_y	1.0	.0	.0	.0	.0	.0
Pitch Moment, M_x	.0	.79	.14	.0	.0	.07
Yaw Angle, ϕ	.0	.92	.01	.0	.0	.07
Frequency = 15.4 (Fore-Aft Bending)						
Side Force, F_x	.26	.05	.66	.0	.0	.03
Thrust, F_y	.79	.05	.16	.0	.0	.0
Pitch Moment, M_x	.77	.06	.17	.0	.0	.0
Yaw Angle, ϕ	.77	.09	.14	.0	.0	.0
Frequency = 3Ω = 23						
Side Force, F_x	.0	.02	.67	.15	.15	.01
Thrust, F_y	.41	.08	.50	.01	.01	.07
Pitch Moment, M_x	.0	.12	.84	.01	.02	.01
Yaw Angle, ϕ	.01	.90	.01	.04	.04	.0
Frequency = 15.9 (Side-to-Side Bending)						
Side Force, F_x	.02	.04	.91	.0	.0	.03
Thrust, F_y	.68	.04	.28	.0	.0	.0
Pitch Moment, M_x	.24	.10	.66	.0	.0	.0
Yaw Angle, ϕ	.47	.34	.19	.0	.0	.0

Table 4.4. Fractional Response Contributions of the Turbulence Inputs for the Mod-G Using the Equilibrium Wake

Response/Input	V_y	$V_{y,x}$	$V_{y,z}$	ε_r	$\bar{\gamma}_r$	Other
Frequency ≃ 0						
Side Force, F_x	.0	.06	.92	.0	.0	.02
Thrust, F_y	1.0	.0	.0	.0	.0	.0
Yaw Moment, M_z	.0	.97	.0	.0	.0	.03
Pitch Moment, M_x	.0	.0	.97	.0	.0	.03
Frequency = 2.69 (Fore-Aft Bending)						
Side Force, F_x	.93	.04	.02	.0	.0	.01
Thrust, F_y	.78	.0	.21	.0	.0	.01
Yaw Moment, M_z	.77	.02	.20	.0	.0	.01
Pitch Moment, M_x	.78	.0	.21	.0	.0	.01
Frequency = 3Ω = 5.5						
Side Force, F_x	.02	.39	.09	.25	.24	.01
Thrust, F_y	.01	.02	.19	.38	.39	.01
Yaw Moment, M_z	.02	.31	.0	.34	.32	.01
Pitch Moment, M_x	.01	.02	.20	.38	.39	.0
Frequency = .89 (Drive Train)						
Side Force, F_x	.0	.08	.90	.0	.0	.02
Thrust, F_y	1.0	.0	.0	.0	.0	.0
Yaw Moment, M_z	.11	.87	.01	.0	.0	.01
Pitch Moment, M_x	.01	.0	.97	.0	.0	.02

when compared to what happens when computing, side force, or yaw and pitch responses using only the single V_y turbulence input. The responses are underestimated by orders of magnitude over a fairly broad frequency range. From these comparisons the inescapable conclusion is that the turbulence gradient terms $v_{y,x}$ and $V_{y,z}$ are just as important as the uniform term V_y, when computing wind turbine structural responses.

Determining the effect of discarding the in-plane turbulence inputs, V_x, V_z, γ_{xz}, ε_r, $\bar{\gamma}_r$, and $\bar{\varepsilon}_{xz}$ can be accomplished by comparing the responses plotted in Figures 4.2 through 4.8, where the effect of all turbulence inputs was included, with the results in Figures 4.13 through 4.18. For example, an overlay of Figure 4.5 and Figure 4.16, which presents the Mod-G side force, shows that there is only a small difference around the frequency 3Ω. From this it is concluded that the in-plane velocity components are not particularly important. In addition, these results suggest that careful study and understanding of small variations in wind direction is not nearly as important as determining the gradient of the longitudinal wind across the rotor disk.

Examining the sensitivity of turbine power output to atmospheric turbulence leads to a somewhat different situation. The power for a three-bladed rigid rotor is only influenced by three turbulence inputs, V_y, γ_{zx} and $\bar{\varepsilon}_{zx}$, as shown by the equations of motion in the Appendix. As explained earlier, the simple structural model used here prevents one from drawing

any firm conclusions concerning the coupling of power fluctuations to any of the other turbulence inputs through the tower motions. Considering the magnitude of these three turbulence inputs shows that the V_y input is the most important, while $\bar{\varepsilon}_{zx}$ is almost certainly unimportant, leaving γ_{zx} as a marginal term.

4.6 Conclusions and Recommendations

On the basis of the work done in this study, the longitudinal turbulence input, V_y, and the two gradients, $V_{y,x}$ and $V_{y,z}$ are of equal importance when computing the dynamic response of wind systems, and these three inputs together comprise the major excitation source for horizontal axis wind turbines. Because of the simplifying assumptions and approximations used in this analysis, it is imperative that the results and the technique be validated with experimental data, prior to use for design.

Although this study only supports the above conclusion for three-bladed stiff rotors, the authors believe that the two gradient terms $v_{y,x}$ and $v_{y,z}$ will be found to be equally important in the dynamic analysis of flexible, or teetering, two-bladed rotors. One reason for this supposition is that the two-bladed rotor will see a turbulence input with a peak at 2Ω caused by the blades rotating through the gradients $V_{y,x}$ and $V_{y,z}$. This will result in a turbulence input spectrum analogous to the one for γ_r, which has a peak at 3Ω as illustrated in Figure 2.11. For the three-bladed rotor, this

only involves the relatively unimportant in-plane velocity gradients, while for the two-bladed rotor it will involve the significant gradients $V_{y,x}$ and $V_{y,z}$.

4.7 References

1. Sullivan, T.L., Miller, D.R. and Speara, D.A., Drive Train Normal Modes Analysis for the ERDA/NASA 100-kilowatt Wind Turbine Generator, NASA TM-73718, July 1977.

2. Martinez-Sanchez, M., Drive Train Dynamics Vol. IV. of Wind Energy Conversion; Massachusetts Institute of Technology, Aeroelastic and Structures Research Laboratory Report ASRL-TR-184-7, 1980.

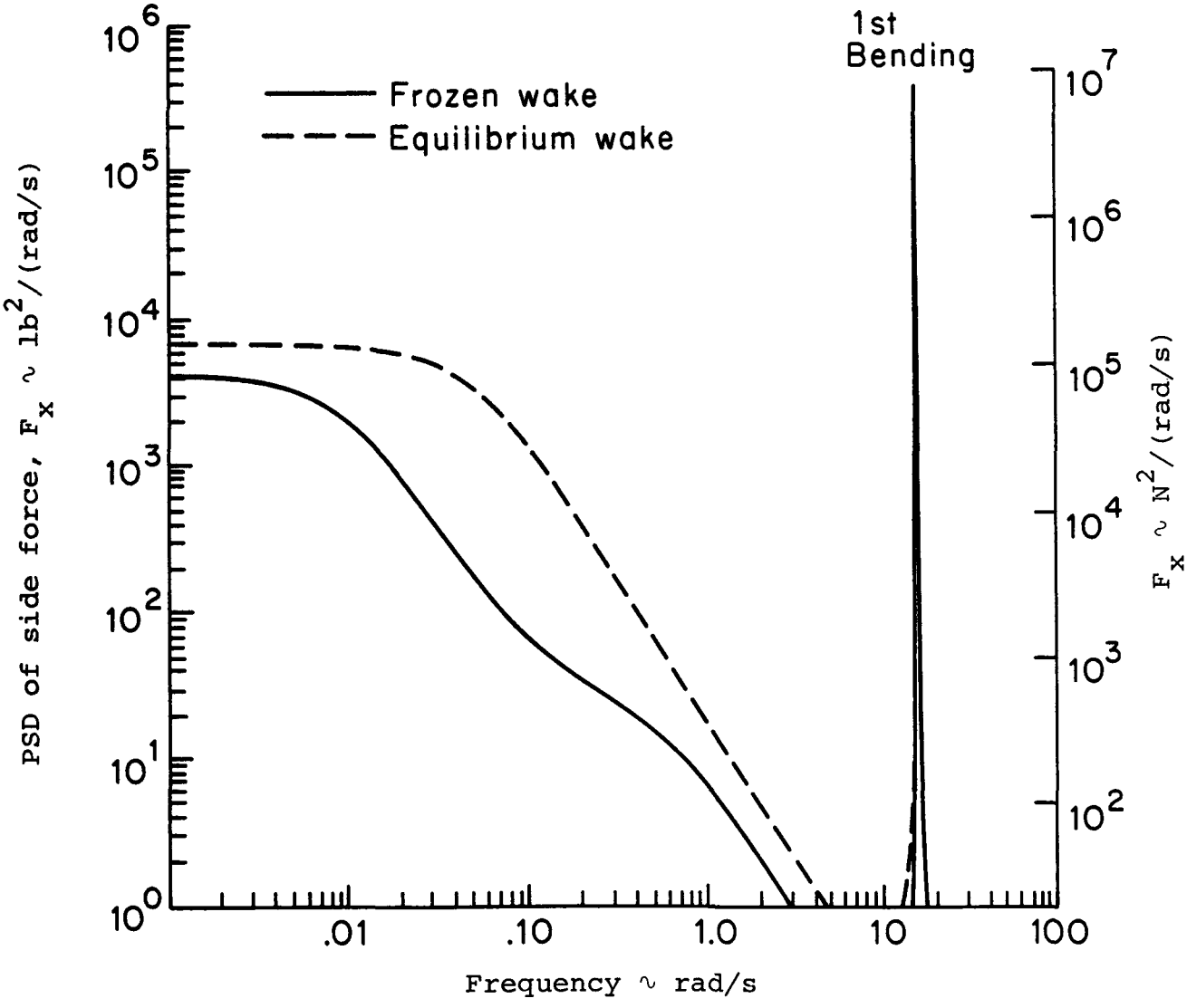

Figure 4.1. Mod-M power spectral density of side force, F_x.

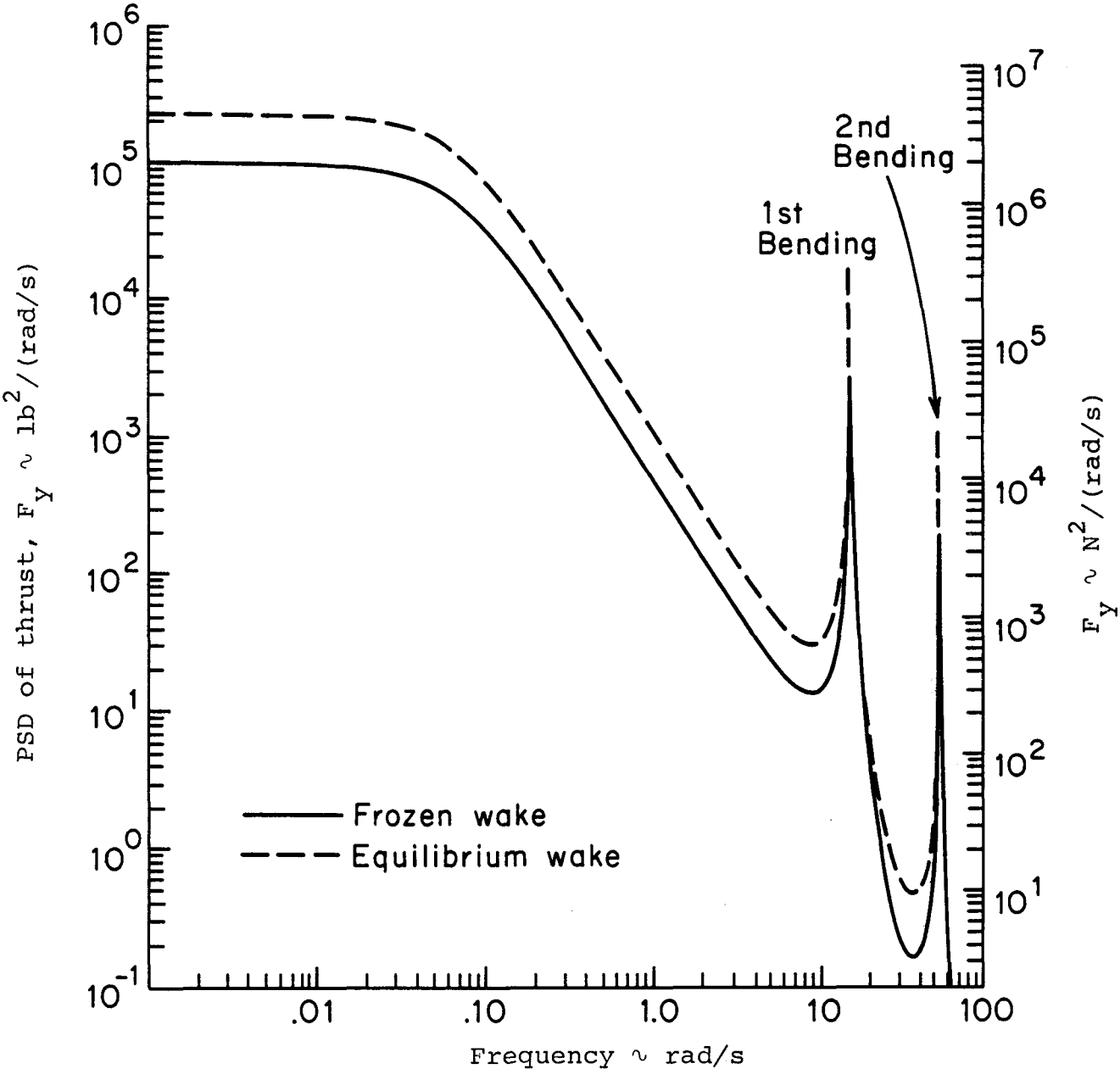

Figure 4.2. Mod-M power spectral density of thrust, F_y.

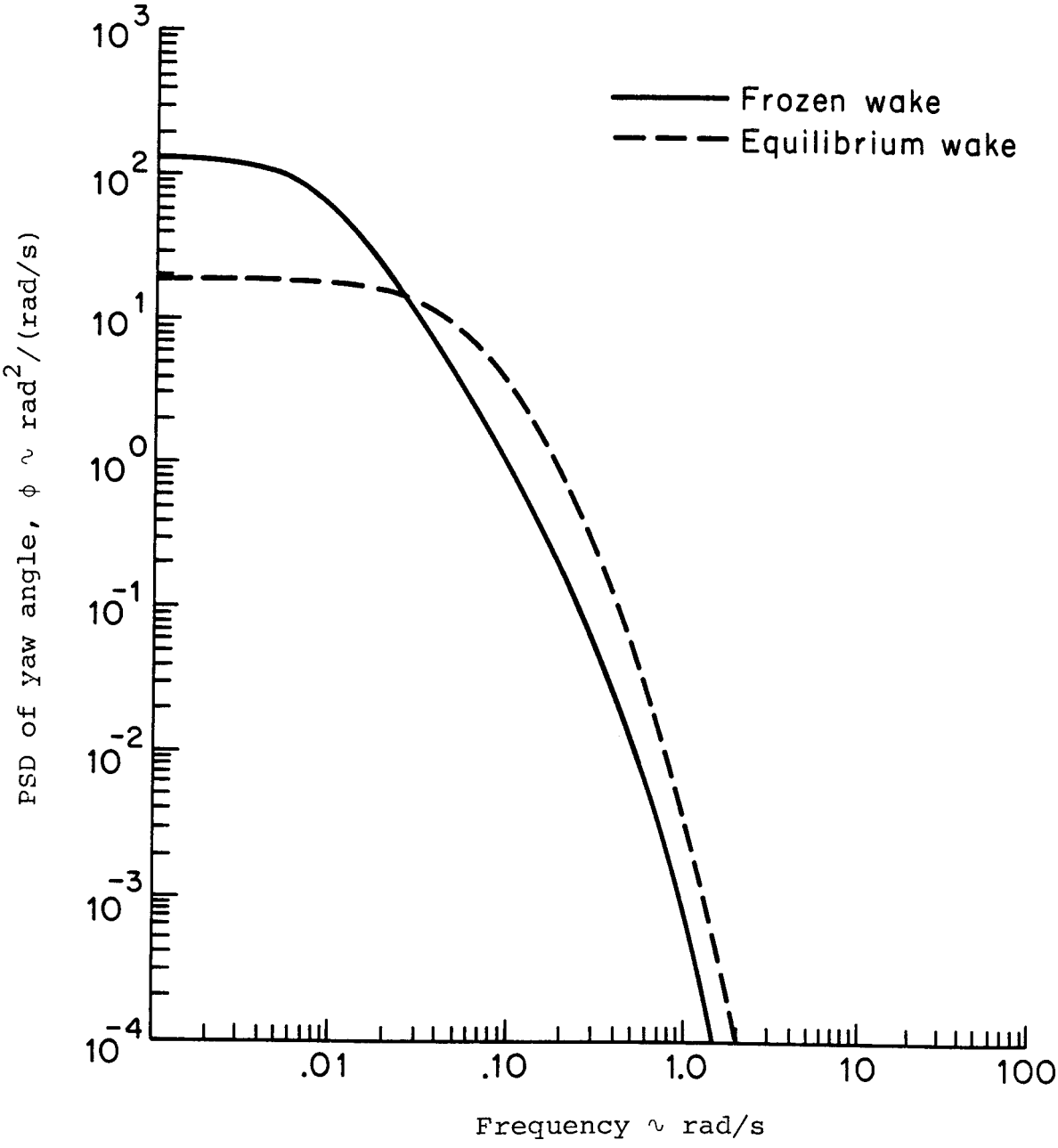

Figure 4.3. Mod-M power spectral density of yaw angle, ϕ.

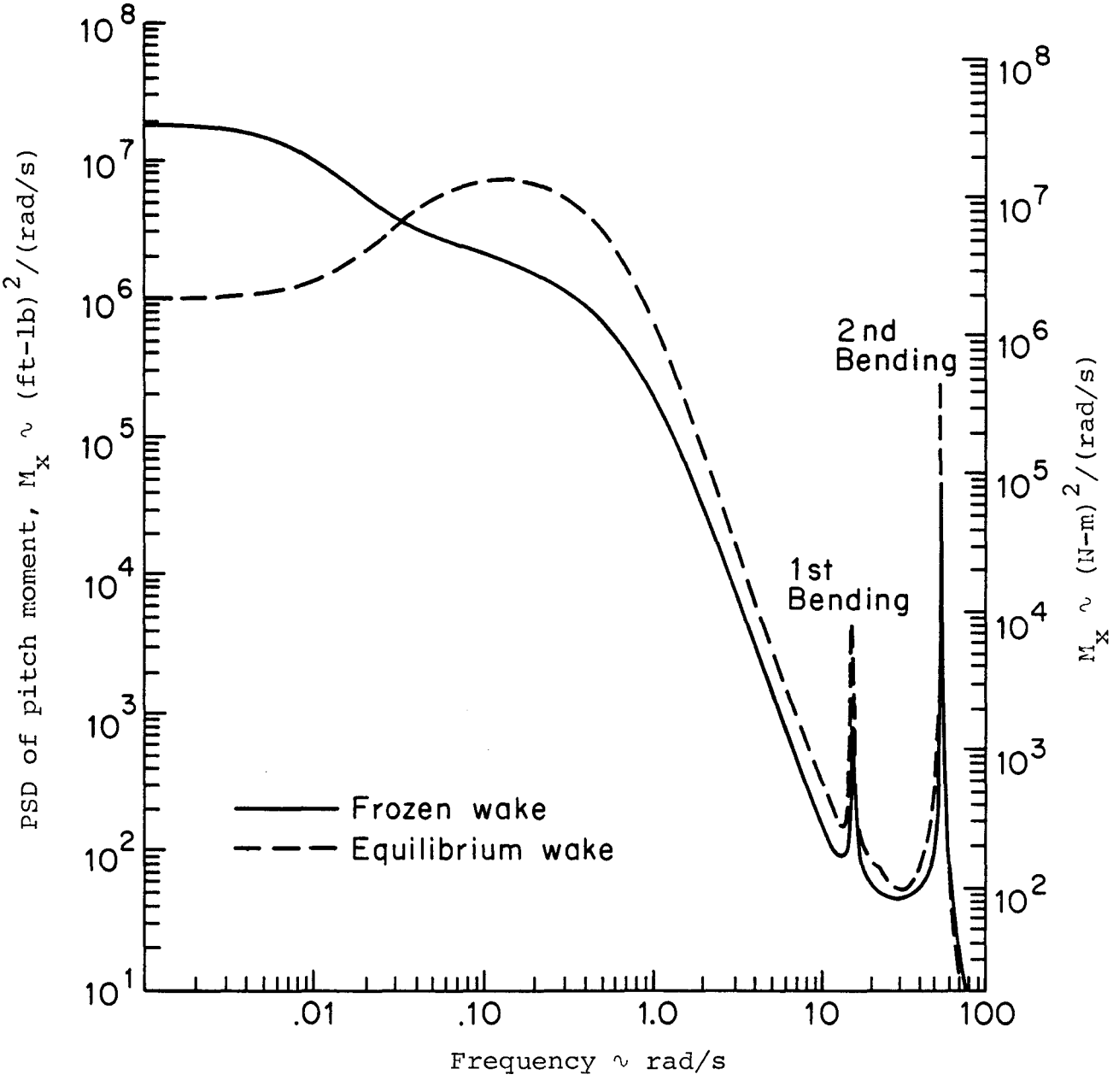

Figure 4.4. Mod-M power spectral density of pitch moment, M_x.

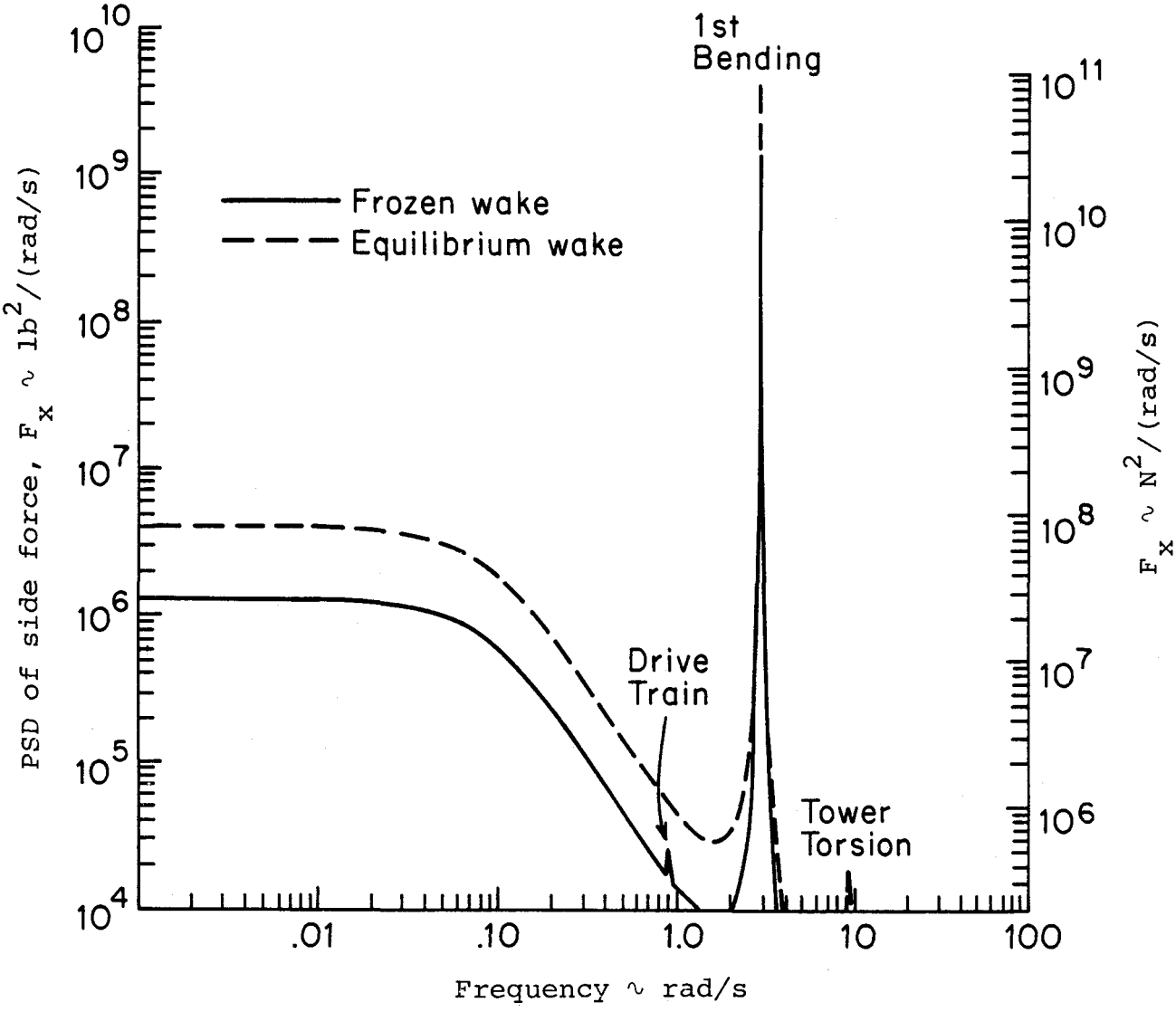

Figure 4.5. Mod-G power spectral density of side force, F_x.

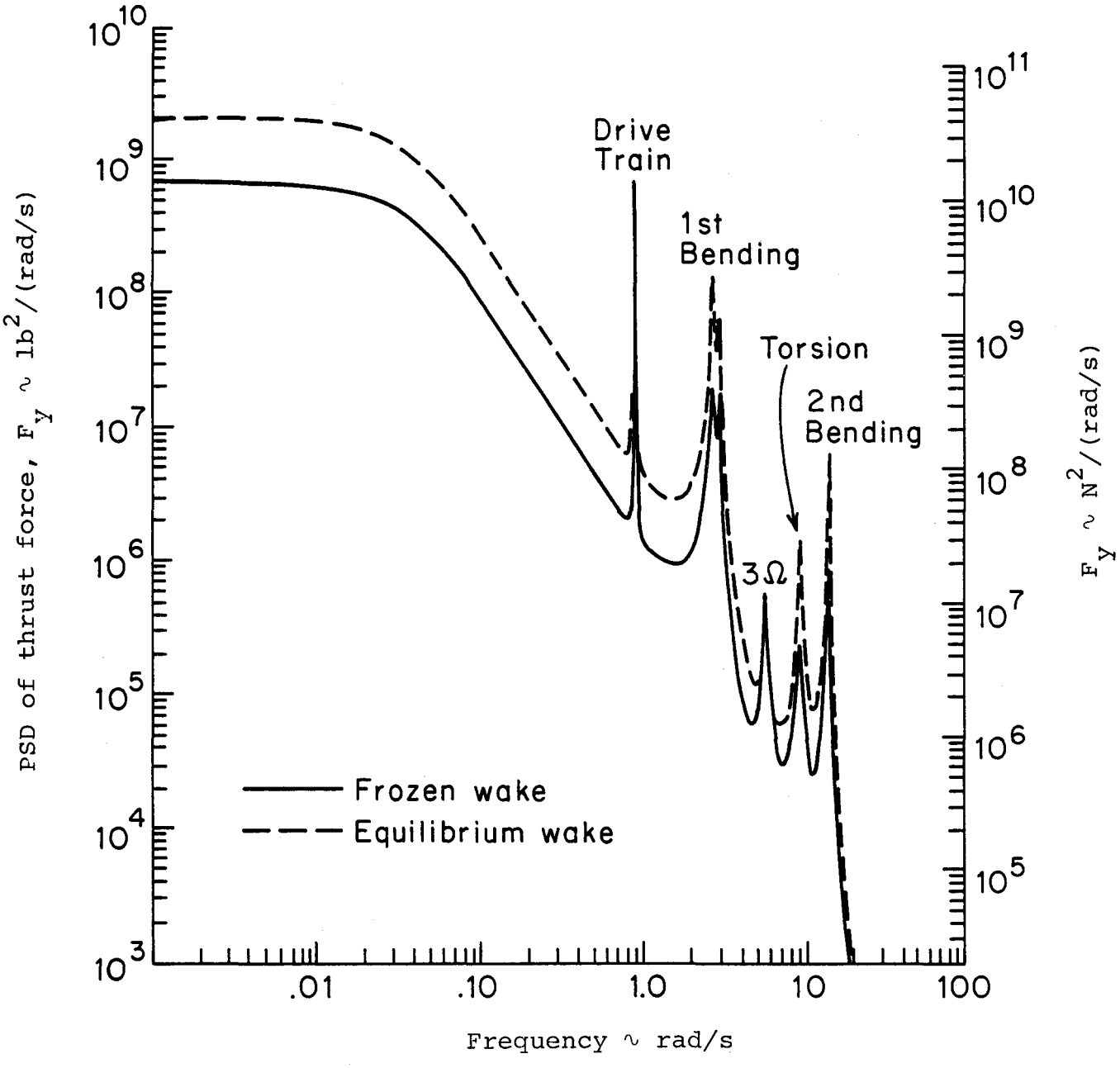

Figure 4.6. Mod-G power spectral density of thrust force, F_y.

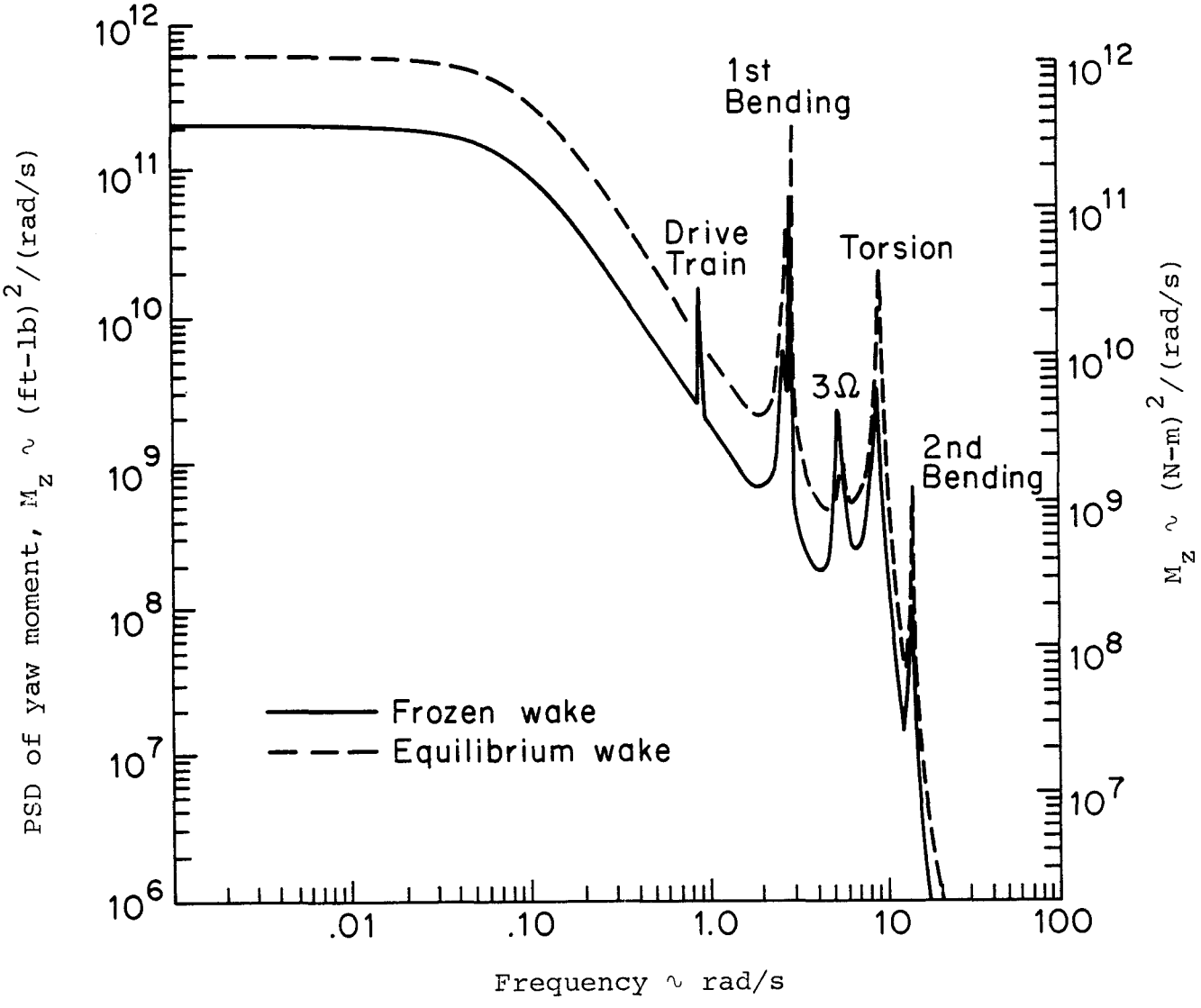

Figure 4.7. Mod-G power spectral density of yaw moment, M_z.

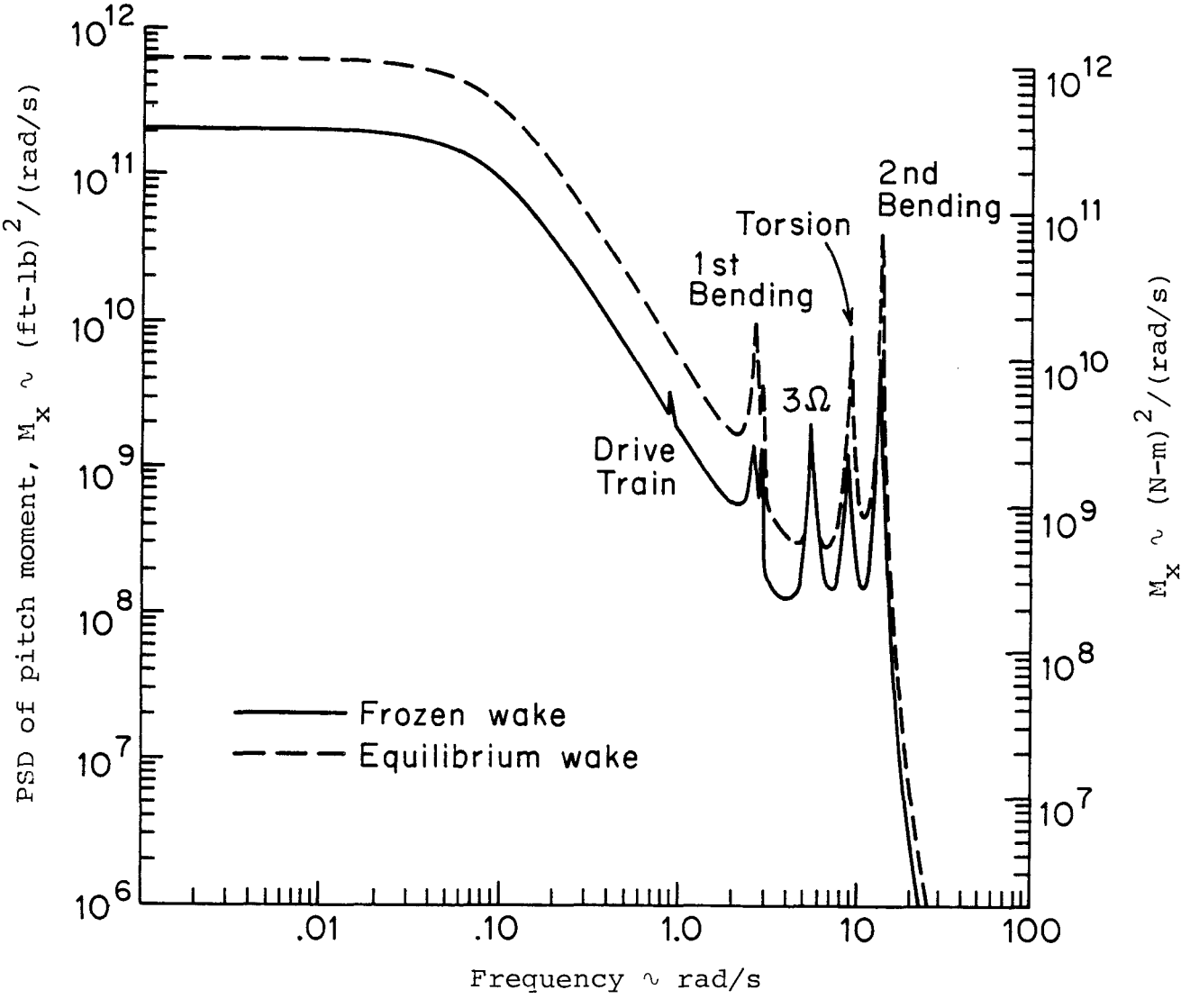

Figure 4.8. Mod-G power spectral density of pitch moment, M_x.

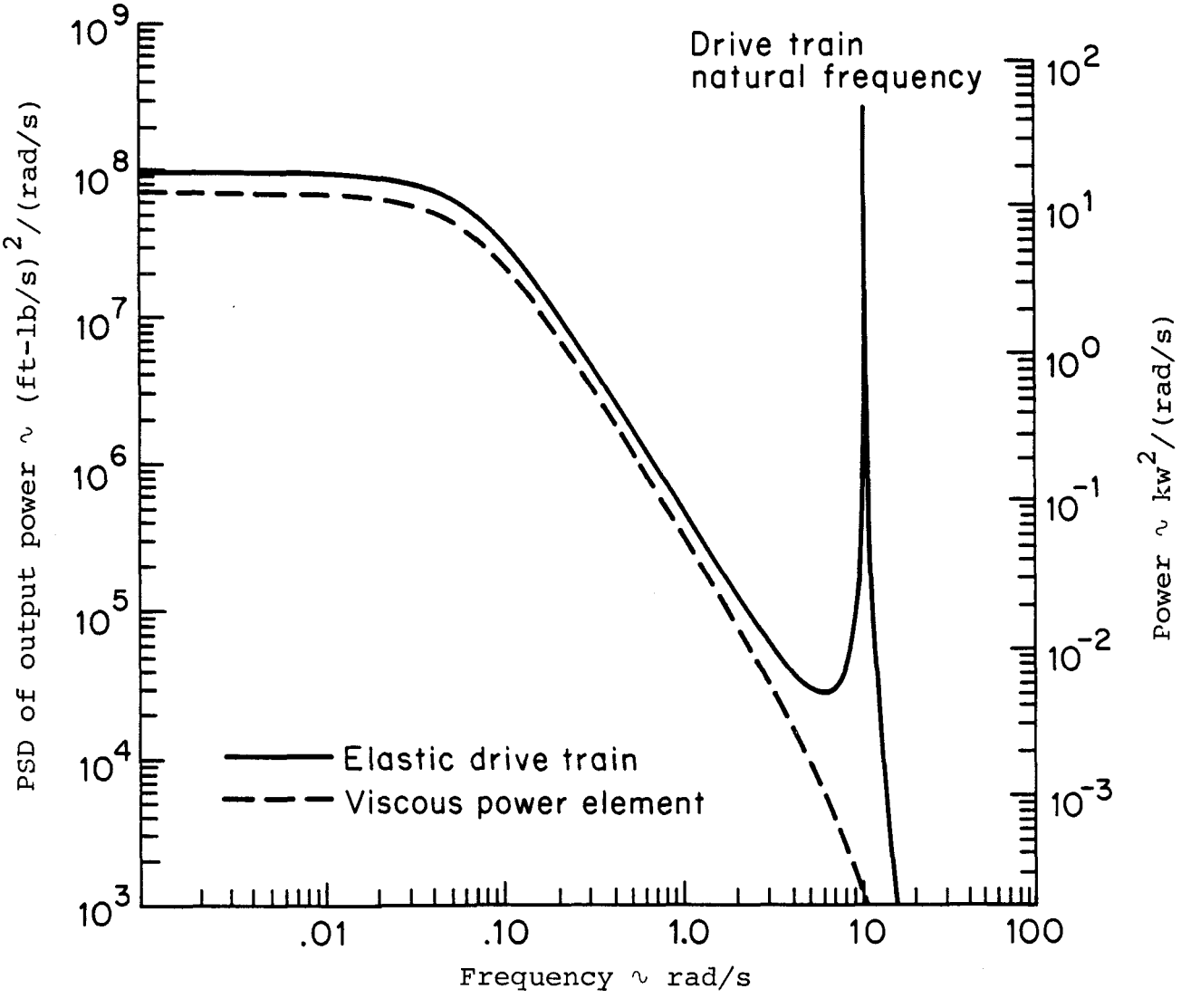

Figure 4.9. Mod-M power spectral density of power output using the frozen wake.

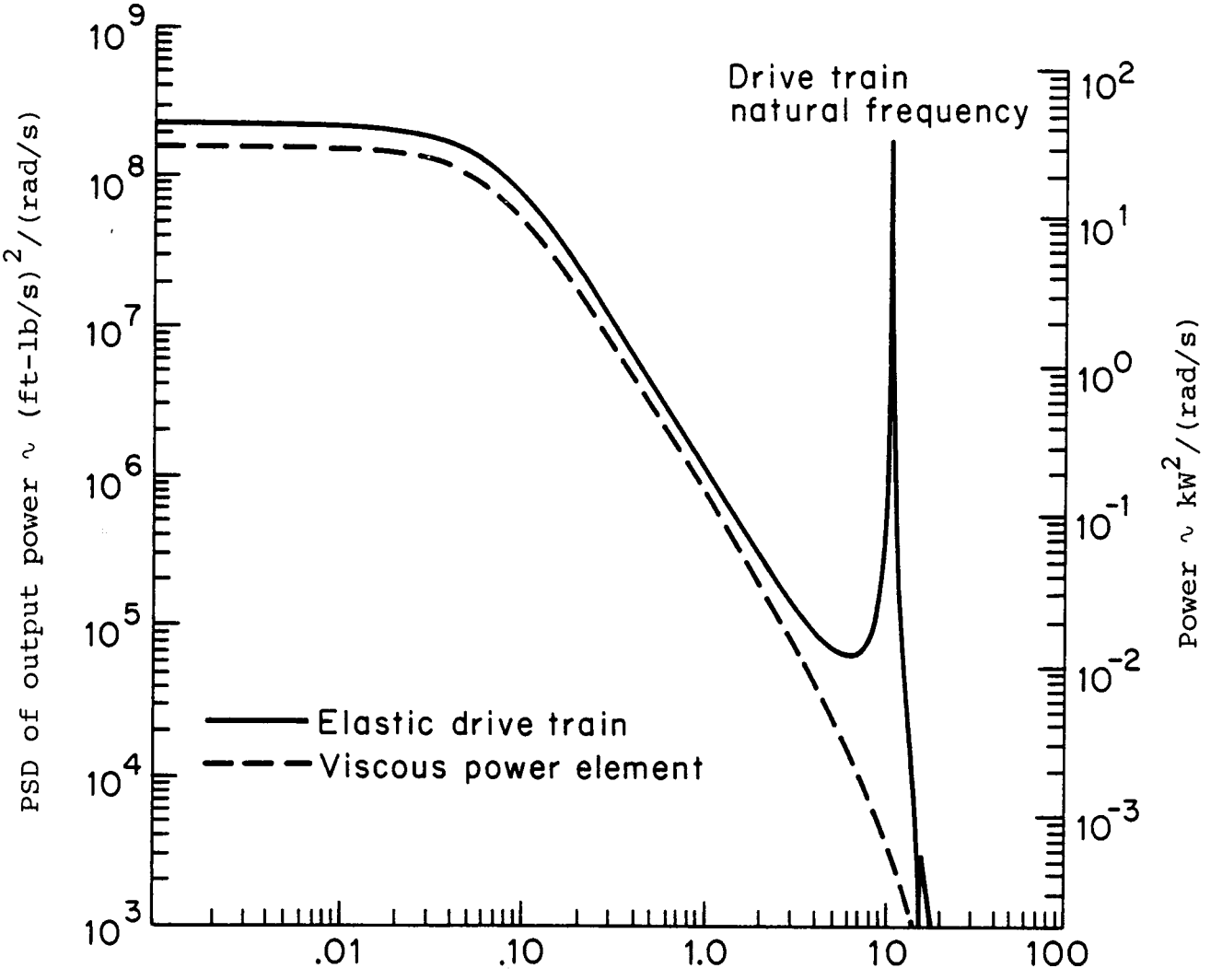

Figure 4.10. Mod-M power spectral density of power output using the equilibrium wake.

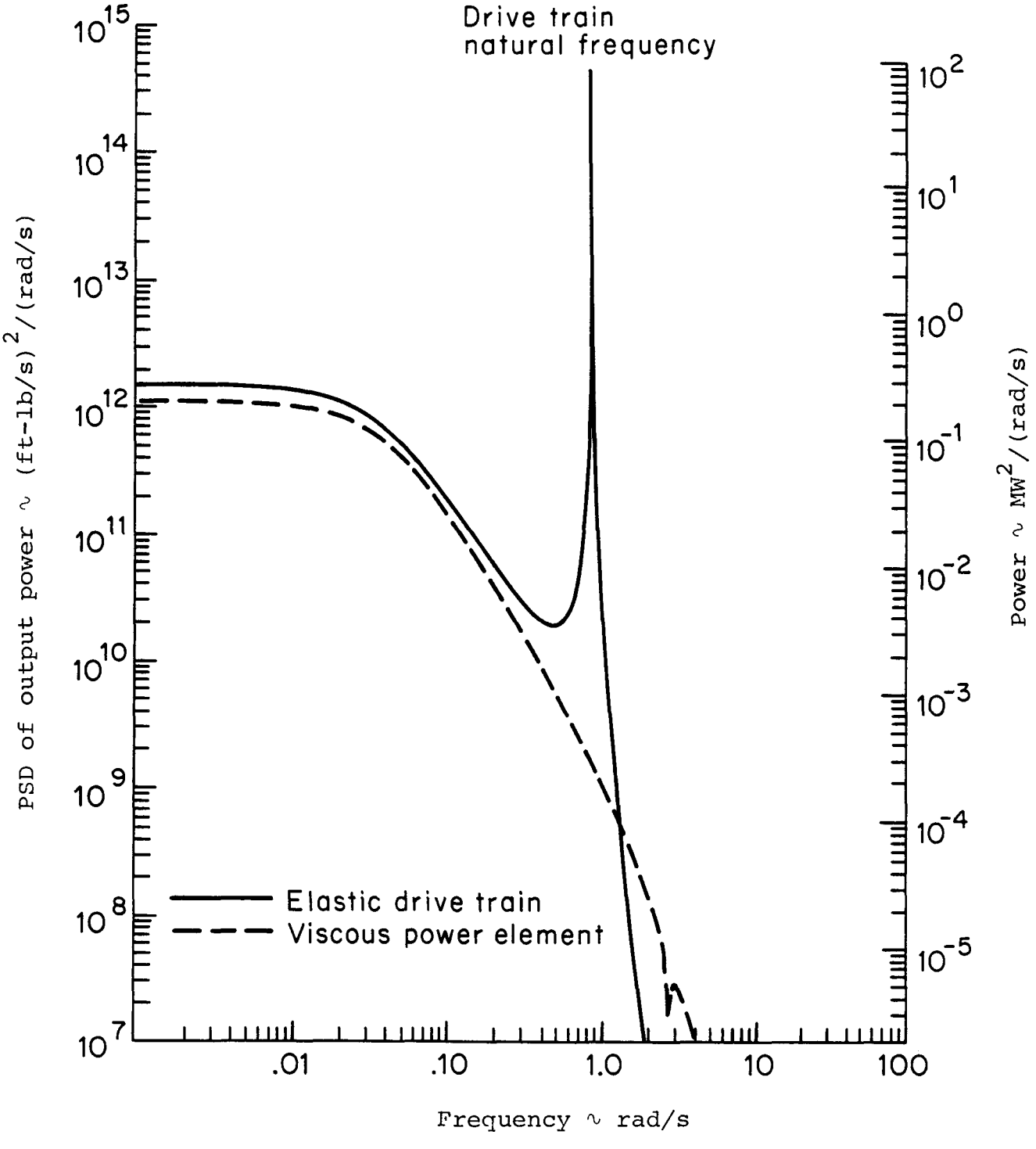

Figure 4.11. Mod-G power spectral density of power output using the frozen wake.

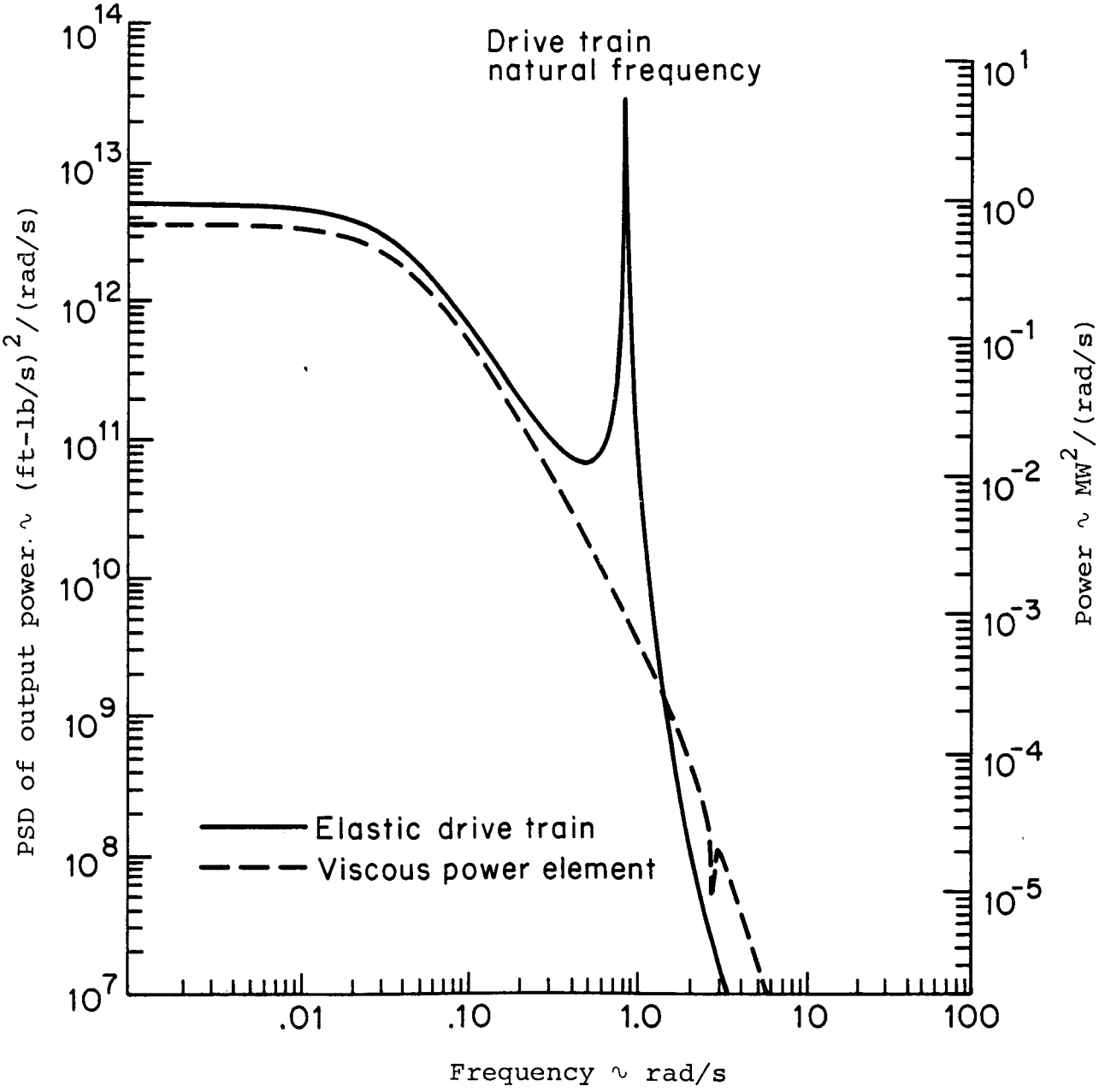

Figure 4.12. Mod-G power spectral density of power output using the equilibrium wake.

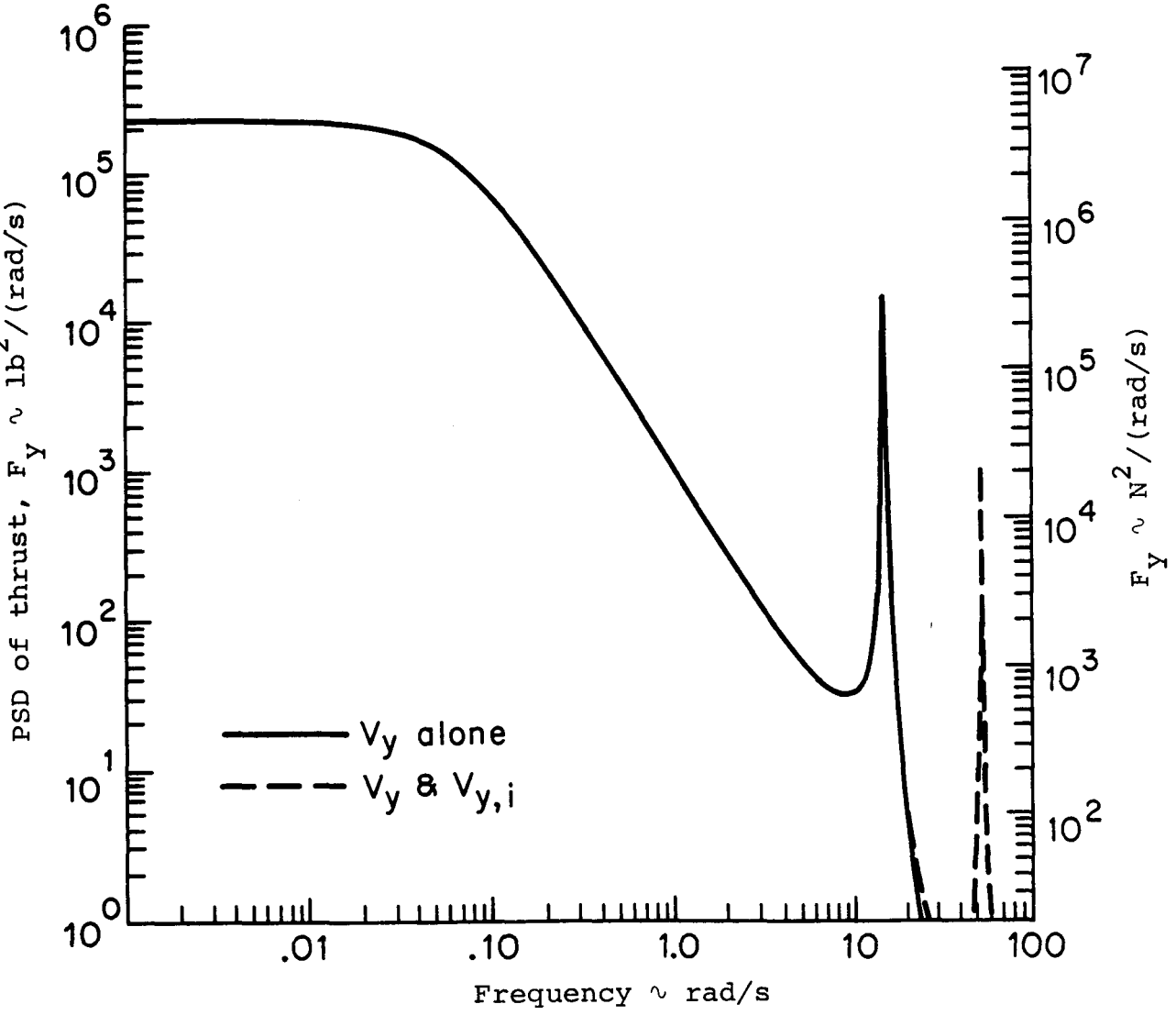

Figure 4.13. The effect of the gradients, $v_{y,x}$ and $v_{y,z}$ on thrust for Mod-M using the equilibrium wake.

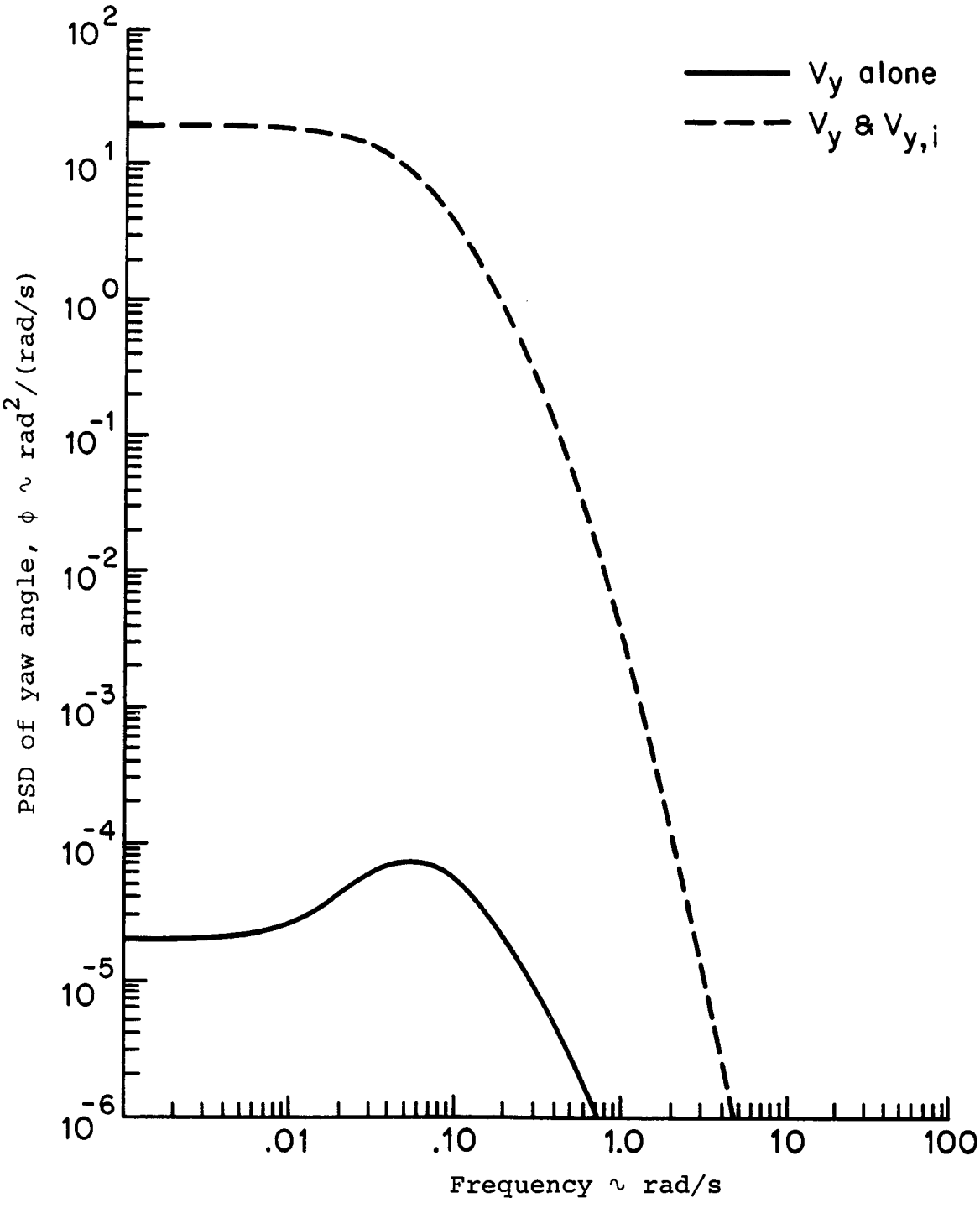

Figure 4.14. The effect of the gradients $v_{y,x}$ and $v_{y,z}$ on yaw angle for Mod-M using the equilibrium wake.

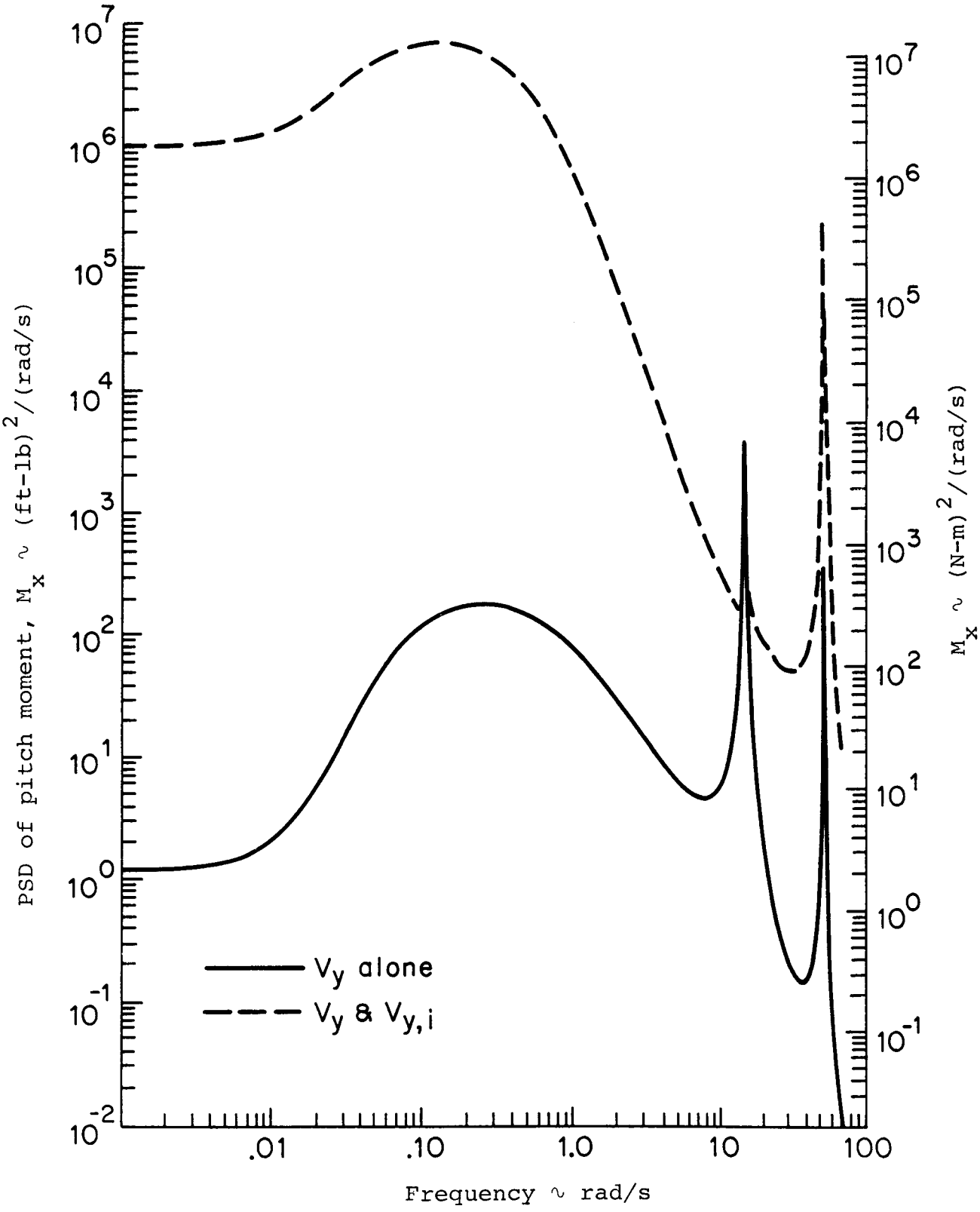

Figure 4.15. The effect of the gradients, $v_{y,x}$ and $v_{y,z}$ on pitch moment for Mod-M using the equilibrium wake.

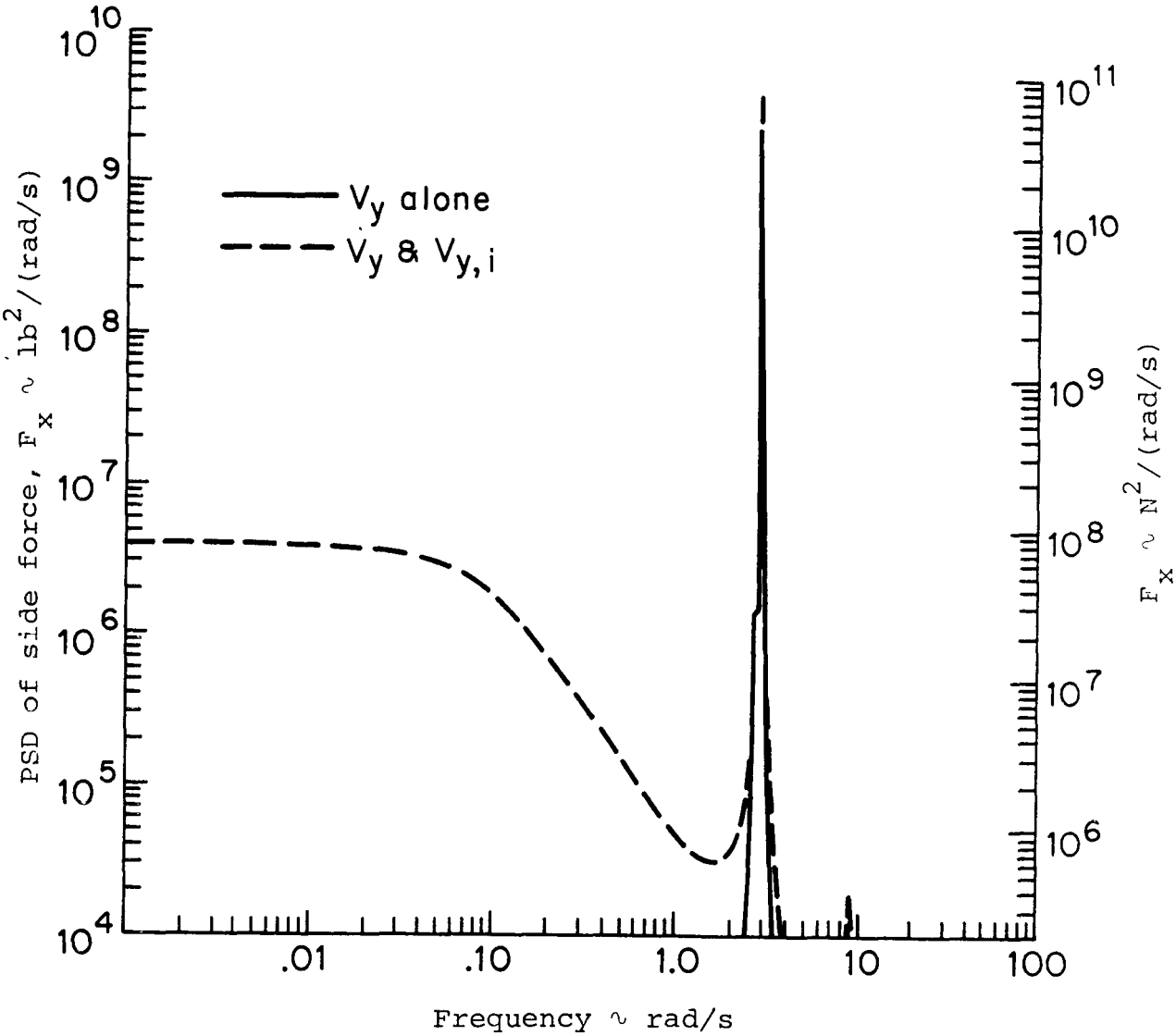

Figure 4.16. The effect of the gradients $v_{y,x}$ and $v_{y,z}$ on the side force for Mod-G using the equilibrium wake.

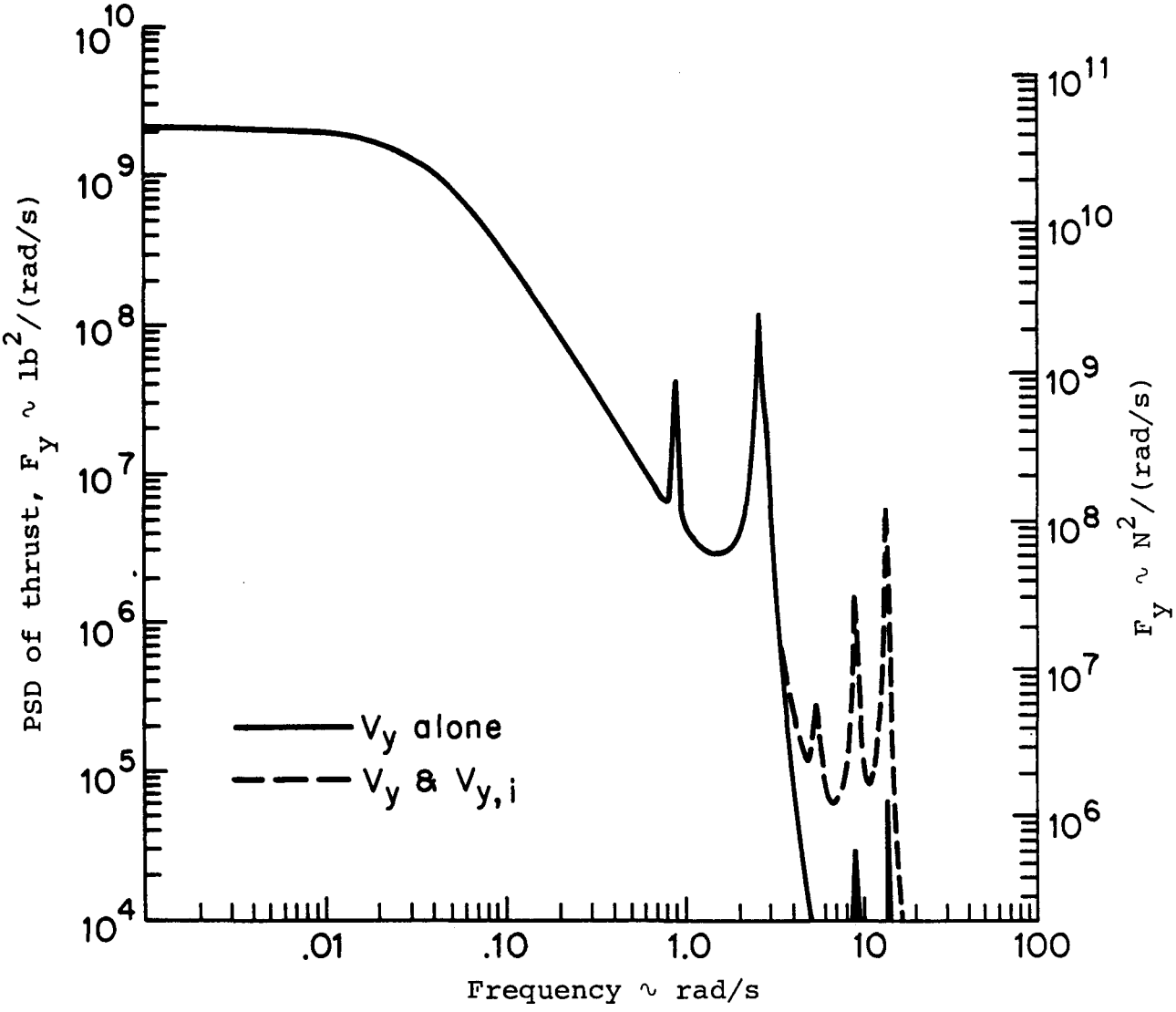

Figure 4.17. The effect of the gradients $v_{y,x}$ and $v_{y,z}$ on thrust for the Mod-G using the equilibrium wake.

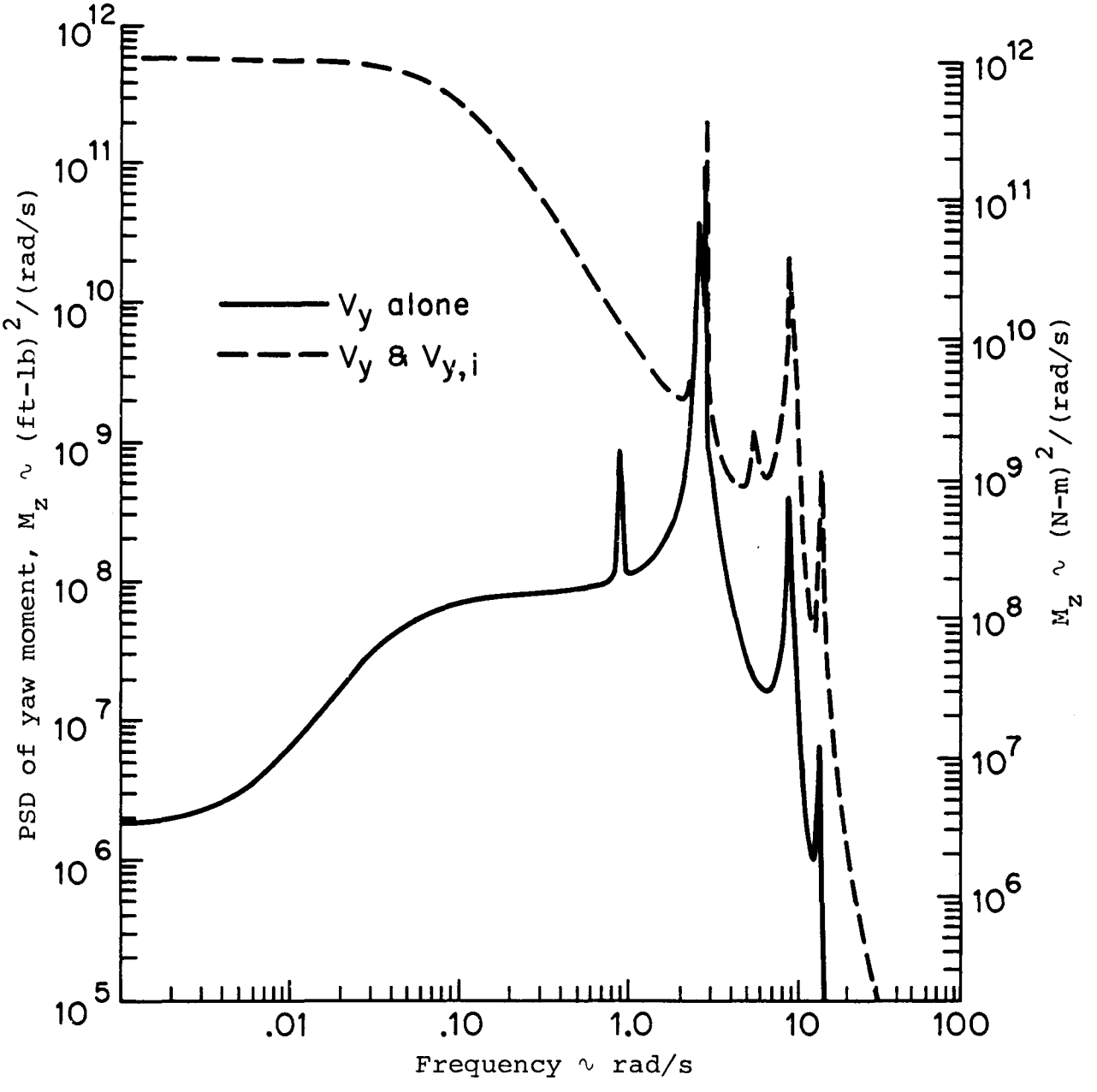

Figure 4.18. The effect of the gradients $v_{y,x}$ and $v_{y,z}$ on yaw moments for Mod-G using the equilibrium wake.

APPENDIX

Turbine System Equations

Governing Equations:

$$\begin{bmatrix} M_{11} & 0 & M_{13} & 0 & 0 \\ 0 & M_{22} & 0 & M_{24} & 0 \\ M_{31} & 0 & M_{33} & 0 & 0 \\ 0 & M_{42} & 0 & M_{44} & 0 \\ 0 & 0 & 0 & 0 & M_{55} \end{bmatrix} \begin{Bmatrix} \ddot{U} \\ \ddot{V} \\ \ddot{\phi} \\ \ddot{\chi} \\ \ddot{\psi} \end{Bmatrix} + \begin{bmatrix} C_{11} & 0 & C_{13} & C_{14} & 0 \\ 0 & C_{22} & 0 & 0 & C_{25} \\ C_{31} & 0 & C_{33} & C_{34} & 0 \\ C_{41} & 0 & C_{43} & C_{44} & 0 \\ 0 & C_{52} & 0 & 0 & C_{55} \end{bmatrix} \begin{Bmatrix} \dot{U} \\ \dot{V} \\ \dot{\phi} \\ \dot{\chi} \\ \dot{\psi} \end{Bmatrix}$$

$$+ \begin{bmatrix} K_{11} & 0 & K_{13} & K_{14} & 0 \\ 0 & K_{22} & 0 & K_{24} & 0 \\ 0 & 0 & K_{33} & K_{34} & 0 \\ 0 & K_{42} & K_{43} & K_{44} & 0 \\ 0 & 0 & 0 & 0 & K_{55} \end{bmatrix} \begin{Bmatrix} U \\ V \\ \phi \\ \chi \\ \psi \end{Bmatrix} = \begin{Bmatrix} 0 \\ T \\ 0 \\ 0 \\ Q \end{Bmatrix}$$

$$+ \begin{bmatrix} F_{11} & 0 & F_{13} & F_{14} & F_{15} & 0 & F_{17} & F_{18} & 0 \\ 0 & F_{22} & 0 & 0 & 0 & F_{26} & 0 & 0 & F_{29} \\ F_{31} & 0 & F_{33} & F_{34} & F_{35} & 0 & F_{37} & F_{38} & 0 \\ F_{41} & 0 & F_{43} & F_{44} & F_{45} & 0 & F_{47} & F_{48} & 0 \\ 0 & F_{52} & 0 & 0 & 0 & F_{56} & 0 & 0 & F_{59} \end{bmatrix} \begin{Bmatrix} V_x \\ V_y \\ V_z \\ V_{y,x} \\ V_{y,z} \\ \gamma_{zx} \\ (\varepsilon_{zx}\cos 3\Omega t + \bar{\gamma}_{zx}\sin 3\Omega t) \\ (-\varepsilon_{zx}\sin 3\Omega t + \bar{\gamma}_{zx}\cos 3\Omega t) \\ \bar{\varepsilon}_{zx} \end{Bmatrix}$$

Inertia Matrix

$M_{11} = m_{11} + m_n + m_r$; $M_{13} = M_{31} = -(m_n + m_r)q$

$M_{22} = m_{22} + m_r + m_n$; $M_{24} = M_{42}$; $M_{33} = m_{33} + I_{zz}$

$M_{44} = m_{44} + I_{xx}$; $M_{55} = I_r$; m_r = mass of rotor ; m_n = mass of nacelle

q = distance from C_L tower to nacelle-rotor C.G. ; I_{xx} and I_{yy} = mass moment of inertia of nacelle-rotor system about x and y axes ; I_r = rotor effective spinning inertia ; m_{ij} = tower inertia coefficients of Eq. (3.4), where for a uniform cantilever tower,

$m_{11} = 99\, m_t/420$, $m_{22} = 156\, m_t/420$, $m_{24} = 22\, m_t L_t/420$

$m_{33} = I_m L_t/3$, $m_{44} = m_t L_t^2/105$, m_t = tower mass , I_m = tower polar inertia

Damping Matrix

$C_{11} = 3f(B_o + \beta_o^2 F_o)/2R\Omega$; $C_{13} = -3f(\bar{a}B_o + \beta_o F_1)/2\Omega$; $C_{14} = -3f(C_1 + \bar{a}\beta_o E_o)/2\Omega$

$C_{22} = 3fF_o/R\Omega$; $C_{25} = -3fE_1/\Omega$; $C_{31} = -3f(\beta_o\{F_1 + B_1^*\} + \bar{a}\{B_o + \beta_o^2 F_o\})/2\Omega$

$C_{33} = 3fR(\{F_2 + \beta_o\bar{a}B_1^*\} + \bar{a}\{\bar{a}B_o + \beta_o F_1\})/2\Omega$; $C_{34} = 3fR(\{E_1\bar{a} + \beta_o C_2^*\} + \bar{a}\{C_1 + \bar{a}\beta_o E_o\})/2\Omega + I_r\Omega$

$C_{41} = 3f(\{E_1 + \beta_o^2 C_1^*\} + \bar{a}\beta_o\{C_o + E_o\})/2\Omega$; $C_{43} = -C_{34}$; $C_{44} = C_{33}$

$C_{52} = 3fC_1/\Omega$; $C_{55} = 3fRB_2/\Omega + C_g$; C_g = Generator torque coefficient

Stiffness Matrix

$K_{11} = k_{11}$; $K_{13} = -3fG_o/2$; $K_{14} = -3f\beta_o H_o/2$; $K_{22} = k_{22}$; $K_{24} = k_{24}$

$K_{33} = k_{33} + 3fR(\beta_o G_1^* + \bar{a}G_o)/2$; $K_{34} = 3fR(H_1 + \beta_o\bar{a}H_o)/2$; $K_{42} = K_{24}$

$K_{43} = -K_{34}$; $K_{44} = k_{44} + 3fR(\beta_o G_1^* + \bar{a}G_o)/2$; k_{55} = Drive train stiffness

where k_{ij} = tower structural stiffnesses from Eq. (3.3), and for a uniform cantilever tower $k_{11} = 3EI/L^3$; $k_{22} = 12EI/L^3$; $k_{24} = 6EI/L^2$; $k_{33} = GJ/L$; $k_{44} = 4EI/L$

Wind Input Matrix

$F_{11} = 3f(B_o + \beta_o^2 F_o)/2R\Omega$; $F_{13} = -3f\beta_o(C_o + E_o)/2R\Omega$; $F_{14} = -3f\beta_o F_1/2\Omega$

$F_{15} = 3fC_1/2\Omega$; $F_{17} = -3f\beta_o(C_1 - E_1)/2\Omega$; $F_{18} = -3f(-B_1 + \beta_o^2 F_1)/2\Omega$

$T = 3fD_o$; $F_{22} = 3fF_o/R\Omega$; $F_{26} = 3fE_1/\Omega$; $F_{29} = -3fF_1\beta_o/\Omega$

$F_{31} = -3f(\beta_o\{F_1 + B_1^*\} + \bar{a}\{B_o + \beta_o^2 F_o\})/2\Omega$; $F_{33} = 3f(\{E_1 + \beta_o^2 C_1^*\} + \bar{a}\beta_o\{C_o + E_o\})/2\Omega$

$F_{34} = 3fR(F_2 + \beta_o\bar{a}F_1)/2\Omega$; $F_{35} = -3fR(\beta_o C_2^* + \bar{a}C_1)/2\Omega$

$F_{37} = -3fR(\{E_2 - \beta_o^2 C_2^*\} - \bar{a}\beta_o\{C_1 - E_1\})/2\Omega$; $F_{38} = 3fR(\beta_o\{F_2 - B_2^*\} + \bar{a}\{-B_1 + \beta_o^2 F_1\})/2\Omega$

$F_{41} = F_{33}$; $F_{43} = -F_{31}$; $F_{44} = F_{35}$; $F_{45} = -F_{34}$; $F_{47} = -F_{38}$; $F_{48} = F_{37}$

$Q = 3fRA_1$; $F_{52} = 3fC_1/\Omega$; $F_{56} = -3fR\,B_2/\Omega$; $F_{59} = -3R\beta_o C_2/\Omega$

where $f = \frac{1}{2}\rho a' R c_t (R\Omega)^2$. The single subscript capitalized coefficients A_n through H_n are integral aerodynamic coefficients of the form

$$A_n = \int_h^R A'(\bar{r})\,\bar{r}^n\,d\bar{r} \qquad \text{where } n = 0,1,2$$

with A' through F' defined as given in Eq. (3.13) for the "frozen wake" or Eq. (3.18) for the "equilibrium wake". In addition, $G'(x) = \lambda B'(x)$ and $H'(x) = \lambda E'(x)$, while the coefficients with stars are $B_n^* = B_n - \bar{h}B_{n-1}$, $C_n^* = C_n - \bar{h}C_{n-1}$ and $G_n^* = G_n - \bar{h}G_{n-1}$, and $\bar{h} = h/R$, $\bar{a} = a/R$.